HSP70 ameliorated neurologic deficits and the neuronal degeneration of spinocerebellar ataxia type 1 (SCA1) transgenic mice, whereas the NIs consisting of mutant ataxin-1 were not reduced (Cummings et al., 2001).

In the present study, we report that overexpression of the inducible form of human HSP70 markedly ameliorated clinical and pathological phenotypes, and that this amelioration was correlated with the reduction of nuclear-localized mutant AR protein complexes in the mouse model of SBMA (Katsuno et al., 2002). Furthermore, the amount of monomeric mutant AR was also significantly reduced in the double-transgenic mice, suggesting that the degradation of mutant AR may have been accelerated by the overexpression of HSP70.

Materials and Methods

Assessment of motor ability. All animal experiments were performed in accordance with the National Institutes of Health *Guide for the Care and Use of Laboratory Animals* and were approved by the Nagoya University Animal Experiment Committee. Motor ability was assessed using an Economex Rotarod (Columbus Instruments, Columbus, OH) on a weekly basis as described previously (Adachi et al., 2001). The period for which a mouse could remain on a rotating axle (diameter, 3.6 cm; speed of rotation, 16 rpm) without falling was measured. Three trials were performed, and the longest duration on the rod was recorded for every mouse. The timer was stopped if the mouse fell from the rod or after an arbitrary limit of 180 sec. Cage activity was measured weekly while each mouse was in a transparent acrylic cage (16 × 30 × 14 cm, width × depth × height) within a soundproofed box as described previously (Katsuno et al., 2002). Spontaneous motor activity was measured by means of an animal behavior system (Neuroscience Inc., Tokyo, Japan), which monitored and counted all spontaneous movements, both vertical and horizontal, including locomotion, rearing, head movements, etc. All counts were automatically totaled and recorded in 24 hr.

Immunohistochemistry. We perfused 20 ml of a 4% paraformaldehyde fixative in 0.1 M phosphate buffer, pH 7.4, through the left cardiac ventricle of mice deeply anesthetized with ketamine–xylazine, postfixed tissues in 10% phosphate-buffered formalin, and processed tissues for paraffin embedding. Then we deparaffinized 4-μm-thick tissue sections, dehydrated with alcohol, and treated for antigen retrieval (Katsuno et al., 2002). For the HSP70 immunohistochemical study, the paraffin sections were pretreated with trypsin (Dako, Glostrup, Denmark) for 20 min at 37°C. The tissue sections were blocked with normal animal serum (1:20) and incubated with mouse anti-expanded polyQ (1:10,000) (1C2; Chemicon, Temecula, CA) and goat polyclonal antibody to HSP70 (1:500) (K-20; Santa Cruz Biotechnology, Santa Cruz, CA). Then the sections were incubated with biotinylated anti-species-specific IgG (Vector Laboratories, Burlingame, CA). Immune complexes were visualized using streptavidin–horseradish peroxidase (Dako) and 3,3′-diaminobenzidine (Dojindo, Kumamoto, Japan) substrate. Sections were counterstained with methyl green.

For double-labeling immunohistochemistry, sections were preincubated with normal horse serum diluted in 0.02 M PBS buffer, pH 7.4, containing bovine serum albumin. The sections were then incubated with goat anti-HSP70 antibody (1:500) (K-20; Santa Cruz) at 4°C overnight, washed with 0.02 M PBS buffer, incubated with biotinylated horse anti-goat IgG, stained with streptavidin–alkaline phosphatase, and visualized with fast red. 1C2 antibody (1:10,000; Chemicon) was subsequently applied to sections at 4°C overnight. After being washed, the sections were incubated with horseradish peroxidase-labeled donkey anti-mouse Ig $F(ab')_2$ (Amersham Biosciences, Buckinghamshire, UK), which had been demonstrated to cross-react with neither goat nor horse sera, and visualized with 3,3′-diaminobenzidine. For double-immunofluorescence staining of the spinal cord, sections were blocked with 5% normal horse serum and then sequentially incubated with K-20 antibody (1:500; Santa Cruz Biotechnology) and 1C2 antibody (1:10,000; Chemicon) at 4°C overnight. After incubation with biotinylated horse anti-goat IgG (Vector Laboratories) for 8 hr at 4°C, the sections were incubated with Alexa-488-conjugated streptavidin (1:400; Molecular Probes, Leiden, The Netherlands) and Alexa-568-conjugated goat anti-mouse IgG (1:1300; Molecular Probes), which had been demonstrated to cross-react with neither goat nor horse sera, for 8 hr at 4°C. The sections were then examined and photographed under a confocal laser scanning microscope (MRC 1024; Bio-Rad, Hercules, CA).

As for the immunohistochemistry of SBMA patients, nine patients with clinicopathologically and genetically confirmed SBMA (age, 51–84 years; mean, 64.3) and three non-neurological controls (age, 51–76 years; mean, 64.0) served as the subjects of the present study. Paraffin-embedded sections of the spinal cord and brain were obtained and examined in the same way as for the transgenic mice.

Quantification of 1C2-positive cells in the spinal cord and muscle. For the assessment of 1C2-positive cells, 4-μm-thick coronal sections of the thoracic spinal cord and gastrocnemius muscle stained by 1C2 antibody (1:10,000; Chemicon) were prepared, and the number of 1C2-positive cells for one mouse was counted using a light microscope with a computer-assisted image analyzer (Luzex FS; Nikon, Tokyo, Japan). For the assessment of 1C2-positive cells in the ventral horn of the spinal cord, 50 consecutive transverse sections of the thoracic spinal cord were prepared, and the 1C2-positive cells present within the ventral horn on every fifth section were counted as described previously (Terao et al., 1996; Adachi et al., 2001). Populations of 1C2-positive cells were expressed as the number per square millimeter. For the assessment of 1C2-positive cells in the muscle, 1C2-positive cells were calculated from counts of >500 fibers in randomly selected areas and were expressed as the number per 100 muscle fibers.

Western blots. We exsanguinated mice under ketamine–xylazine anesthesia and snap-froze their tissues with powdered CO_2 in acetone. Frozen tissue (0.1 gm wet weight) was homogenized in 1000 μl of lysis buffer (50 mM Tris-HCl, pH 8.0, 150 mM NaCl, 1% NP-40, 0.5% deoxycholate, and 0.1% SDS with 1 mM PMSF and aprotinin at 6 μg/ml). Homogenates were spun at 2500 × *g* for 15 min at 4°C. The protein concentration of the supernatant was determined using detergent-compatible protein assay (Bio-Rad). Each lane on a 5–20% SDS-PAGE gel was loaded with protein (200 μg for the spinal cord and 80 μg for the muscle from the supernatant fraction), which was transferred to Hybond-P membranes (Amersham Biosciences) using 25 mM Tris, 192 mM glycine, 0.1% SDS, and 10% methanol as transfer buffer. Kaleidoscope prestained standards were used as size markers (Bio-Rad). Proteins were then transferred to Hybond-P membranes, which were subsequently blocked in 5% milk in TBS containing 0.05% Tween 20 and incubated with appropriate primary antibodies using standard techniques. Primary antibodies were used at the following concentrations: rabbit anti-AR antibody (1:1000 N-20; Santa Cruz Biotechnology); mouse anti-HSP70/heat shock cognate 70 (HSC70) antibody (1:5000, W-27; Santa Cruz Biotechnology). We performed second antibody probing and detection using the ECL+plus kit (Amersham Biosciences). The HRP-conjugated secondary antibodies used were anti-rabbit Ig $F(ab')_2$ and anti-mouse Ig $F(ab')_2$ (1:5000; Amersham Biosciences). Nuclear and cytoplasmic fractions were extracted with a NE-PER Nuclear and Cytoplasmic Extraction Reagents Kit according to the protocol of the manufacturer (Pierce, Rockford, IL). Each lane on a 5–20% SDS-PAGE gel was loaded with 200 μg of protein for the spinal cord and 80 μg for the muscle from each fraction. Immunoprecipitation was performed using 1 mg of the total protein lysate, 10 μl of protein G–Sepharose (Amersham Biosciences), and 5 μl of anti-AR antibody (N-20; Santa Cruz Biotechnology). Protein was eluted from beads by boiling for 3 min in 10 μl of elution buffer (50 mM Tris-HCl, pH 6.8, 2% SDS, 60 μl/ml 2-mercaptoethanol, and 10% glycerol). The elutes were loaded on SDS–polyacrylamide gels. Blots were sequentially probed with goat anti-HSP70 antibody (K-20; Santa Cruz Biotechnology).

The signal intensity was analyzed using the NIH Image program (version 1.62). Relative signal intensity was computed as the signal intensity of each sample divided by that of the AR-97Q/HSP70$^{(-/-)}$ mice.

Filter-trap assay. Filtration of proteins through a 0.2 μm cellulose acetate membrane (Sartorius AG, Goettingen, Germany) was performed using a slot-blot apparatus (Bio-Rad). The membranes were washed

three times with TBS buffer and supported by three pieces of filter paper (Bio-Rad). We also put 0.45 μm nitrocellulose membrane (Bio-Rad) under the cellulose acetate membrane to capture the monomeric AR protein passing through this membrane. Samples of protein (200 μg) for the spinal cord and for the muscle (80 μg) were prepared in a final volume of 200 μl in lysis buffer, loaded, and gently vacuumed. Membranes were washed three times with TBS containing 0.05% Tween 20. Slot-blots were probed as described for Western blots.

Statistical analysis. We analyzed data using the unpaired *t* test and log-rank test from Statview software version 5 (Hulinks, Tokyo, Japan).

Results

Nondeleterious effects of HSP70 overexpression and generation of double-transgenic mice

Because HSP70s have a wide variety of functions, we examined whether the overexpression of HSP70 under the control of the human β-actin promoter has deleterious effects on phenotypes in mice (Plumier et al., 1995). Motor function in the mice with HSP70 overexpression was not affected; a Rotarod task until 40 weeks revealed no impairment in either hemizygous or homozygous transgenic mice overexpressing HSP70 (data not shown). Histological examination at 40 weeks of age did not show any detectable effect on the neuronal cell morphology and population and on the muscular structure in the overexpression of human HSP70 alone (data not shown). These studies indicated that the overexpression of human HSP70 alone does not impair neuronal development and motor function.

To determine whether the overexpression of human HSP70 could ameliorate the disease phenotype of the SBMA transgenic mouse model, we crossed the mice expressing full-length human AR with 97-polyQ tract (AR-97Q mice, 4–6 line) (Katsuno et al., 2002) with mice that overexpress human HSP70 under the control of the human β-actin promoter (Plumier et al., 1995). The SBMA model (AR-97Q mice) shows small body size, short lifespan, progressive muscle atrophy and weakness, and reduced cage activity (Katsuno et al., 2002). Because the phenotypes of these SBMA transgenic mice are markedly pronounced in male transgenic mice similarly to SBMA patients (Katsuno et al., 2002), we used male transgenic mice in this study. We generated the AR-97Q/HSP70$^{(tg/tg)}$ mice as homozygotes and the AR-97Q/HSP70$^{(tg/-)}$ mice as hemizygotes, as well as the AR-97Q/HSP70$^{(-/-)}$ mice as a control transgenic mouse line. The SBMA transgene expression was at the hemizygous level in all AR-97Q/HSP70 double-transgenics.

Human HSP70 overexpression ameliorates motor phenotypes of SBMA transgenic mice

To determine whether HSP70 overexpression has an ameliorative effect on the motor phenotypes, we performed the Rotarod task and the measurement of locomotor cage activity by infrared sensor system with the double-transgenic mice (Fig. 1*A*,*B*). The AR-97Q/HSP70$^{(-/-)}$ mice showed motor impairment on the Rotarod task as early as 9 weeks after birth; by 12 weeks and 25 weeks of age they began to show significant impairment compared with AR-97Q/HSP70$^{(tg/-)}$ mice ($p < 0.05$) and AR-97QHSP70$^{(tg/tg)}$ mice ($p < 0.001$), respectively. (Fig. 1*A*). Although both the AR-97Q/HSP70$^{(tg/tg)}$ and AR-97Q/HSP70$^{(tg/-)}$ mice performed better than the AR-97Q/HSP70$^{(-/-)}$ mice, the AR-97Q/HSP70$^{(tg/tg)}$ mice were on the rod longer than the AR-97Q/HSP70$^{(tg/-)}$ mice during the trial. The locomotor cage activity of the AR-97Q/HSP70$^{(-/-)}$ mice was also significantly decreased at 21 weeks in comparison with the other two double-transgenics ($p < 0.05$) (Fig. 1*B*). No lines were distinguishable in terms of body weight at birth. The AR-97Q/HSP70$^{(-/-)}$ mice lost weight significantly earlier than the AR-97Q/HSP70$^{(tg/tg)}$ mice ($p < 0.01$) (Fig. 1*C*). The survival rate was significantly more prolonged in the AR-97Q/HSP70$^{(tg/-)}$ and AR-97Q/HSP70$^{(tg/tg)}$ mice than in the AR-97Q/HSP70$^{(-/-)}$ mice ($p < 0.01$ and $p < 0.005$, respectively) (Fig. 1*D*). The affected AR-97Q/HSP70$^{(-/-)}$ mice exhibited motor weakness, with dragging of the legs or short steps, whereas the AR-97Q/HSP70$^{(tg/tg)}$ mice showed almost normal ambulation and the AR-97Q/HSP70$^{(tg/-)}$ mice only

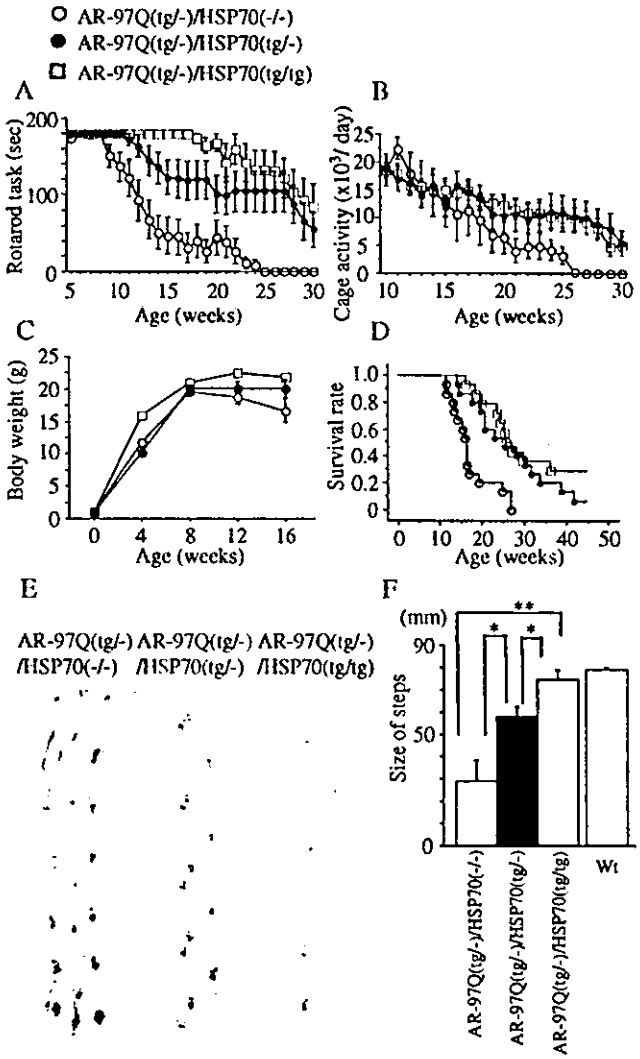

Figure 1. Effects of human HSP70 overexpression on the symptomatic phenotypes of male AR-97Q mice. Rotarod task (*A*; $n = 10$), cage activity (*B*; $n = 10$), body weight (*C*; $n = 12$), and survival rate (*D*; $n = 14$) of the AR-97Q/HSP70$^{(-/-)}$, AR-97Q/HSP70$^{(tg/-)}$, and AR-97Q/HSP70$^{(tg/tg)}$ mice. All parameters were significantly different among AR-97Q/HSP70$^{(-/-)}$ mice, AR-97Q/HSP70$^{(tg/tg)}$, and AR-97Q/HSP70$^{(tg/-)}$ mice ($p < 0.001$, $p < 0.05$, $p < 0.05$, and $p < 0.005$, respectively). AR-97Q mice overexpressing human HSP70 lasted longer on the Rotarod and showed higher cage activity than AR-97Q/HSP70$^{(-/-)}$ mice. The AR-97Q/HSP70$^{(-/-)}$ mice lost weight earlier than the other two double-transgenics. Survival was prolonged in AR-97Q/HSP70$^{(tg/-)}$ and AR-97Q/HSP70$^{(tg/tg)}$ mice compared with AR-97Q/HSP70$^{(-/-)}$ mice. *E*, Footprints of representative 16-week-old AR-97Q/HSP70$^{(-/-)}$, AR-97Q/HSP70$^{(tg/-)}$, and AR-97Q/HSP70$^{(tg/tg)}$ mice. Front paws are indicated in *red* and hindpaws in *blue*. AR-97Q/HSP70$^{(-/-)}$ mice exhibit motor weakness, with dragging of the legs; AR-97Q/HSP70$^{(tg/tg)}$ mice walk almost normally; and AR-97Q/HSP70$^{(tg/-)}$ mice walk with somewhat short steps. *F*, The size of steps was measured in 16-week-old AR-97Q/HSP70$^{(-/-)}$, AR-97Q/HSP70$^{(tg/-)}$, and AR-97Q/HSP70$^{(tg/tg)}$ mice ($n = 4$), respectively. Each column shows an average of steps of the hindpaw. AR-97Q/HSP70$^{(tg/-)}$ and AR-97Q/HSP70$^{(tg/tg)}$ mice walked with significantly longer steps than AR-97Q/HSP70$^{(-/-)}$ mice. $^{*}p < 0.05$; $^{**}p < 0.01$. Error bars indicate SD. *Wt*, Wild type.

somewhat short steps (Fig. 1*E*). The AR-97Q/HSP70$^{(tg/-)}$ and AR-97Q/HSP70$^{(tg/tg)}$ mice showed significantly longer steps than the AR-97Q/HSP70$^{(-/-)}$ mice (Fig. 1*F*). Although both the AR-97Q/HSP70$^{(tg/tg)}$ and AR-97Q/HSP70$^{(tg/-)}$ mice showed ameliorated phenotypic expressions, the AR-97Q/HSP70$^{(tg/tg)}$ mice were better than the AR-97Q/HSP70$^{(tg/-)}$ mice in most of the parameters, suggesting that the improved motor phenotype depended on the HSP70 expression level rather than on the genetic background.

Expression levels of HSP70 in double-transgenic mice

We examined whether the AR-97Q/HSP70 double-transgenic mice express increased levels of the HSP70 protein in the spinal cord and skeletal muscle. Immunohistochemical studies of double-transgenic mice stained with the specific antibody for HSP70 confirmed that spinal neurons and muscular cells expressed the HSP70 (Fig. 2*A–C*). The HSP70 was diffusely distributed to the nuclei and occasionally formed various-sized NIs (Fig. 2*A–C*). Glial cells also showed diffuse nuclear staining and NIs of HSP70 protein (data not shown). Western blot analysis revealed that the HSP70 expression level was fivefold greater in the AR-97Q/HSP70$^{(tg/-)}$ mice and 10-fold greater in the AR-97Q/HSP70$^{(tg/tg)}$ mice than endogenous HSP70 in the AR-97Q/HSP70$^{(-/-)}$ mice in the spinal cord and muscle (Fig. 2*D*). The AR-97Q transgene expression did not alter HSP70 expression levels in the spinal cord of the wild-type and HSP70$^{(tg/tg)}$ mice, whereas the AR-97Q transgene expression increased HSP70 levels in the muscle, suggesting that the stress-induced response is different between the spinal cord and the skeletal muscle (Fig. 2*D*). Absence of the stress-induced response was also demonstrated in the nervous system of the other polyQ disease model mice (Jana et al., 2000; Cummings et al., 2001). The nuclear fraction of the spinal cord and muscle surely contained an increased amount of HSP70 in the double-transgenic mice. The amount of HSP70 in the nuclear fraction was most abundant in the AR-97Q/HSP70$^{(tg/tg)}$ mice (Fig. 2*E*). The increased HSP70 was coimmunoprecipitated with mutant AR, suggesting that HSP70 directly binds to the mutant AR protein (Fig. 2*F*).

Colocalization of HSP70 with mutant AR in the nuclei

We evaluated the colocalization of HSP70 and mutant AR in the AR-97Q/HSP70 double-transgenic mice. We performed double-labeling immunohistochemistry and immunofluorescence double-staining with two primary antibodies: goat anti-HSP70 and mouse anti-expanded polyQ (1C2). These double-immunostaining studies revealed that HSP70 (Fig. 3*A,C*) and mutant AR (Fig. 3*B,D*) present diffusely in the nuclei and colocalize each other (Fig. 3*B,E*) in the spinal anterior horn neurons of the AR-97Q/HSP70$^{(tg/tg)}$ mice. We also determined that such diffuse staining of HSP70 in the nuclei was also present in the spinal neurons of SBMA patients (Fig. 3*F,J*). Immunofluorescence double-staining with anti-HSP70 and anti-expanded polyQ antibodies revealed that the endogenous HSP70 (Fig. 3*G,K*) and mutant AR (Fig. 3*H,L*) were colocalized on the NI (Fig. 3*I*) and diffusely in the nuclei (Fig. 3*M*) in the spinal cord neurons of SBMA patients, suggesting that the endogenous HSP70 preferentially coexists with mutant AR and exerts its function in the nuclei of SBMA patients as well.

Overexpression of HSP70 decreases the nuclear-localized mutant AR

An immunohistochemical study for mutant AR using 1C2 antibody showed a marked reduction in diffuse nuclear staining and NIs in the AR-97Q/HSP70$^{(tg/-)}$ or the AR-97Q/HSP70$^{(tg/tg)}$ mice compared with the AR-97Q/HSP70$^{(-/-)}$ mice in the spinal motor neurons (Fig. 4*A–C*) and muscles (Fig. 4*D–F*). The AR-97Q/HSP70$^{(-/-)}$ mice showed intense and frequent 1C2 staining in the nuclei (Fig. 4*A,D*), whereas the 1C2 staining was infrequent

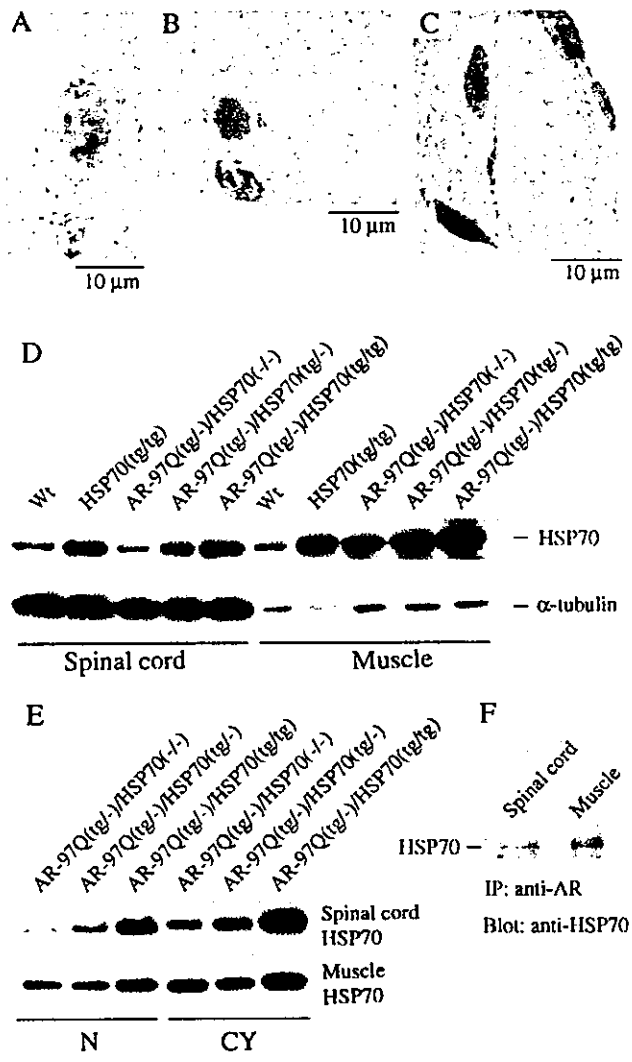

Figure 2. Increased HSP70 expression in double-transgenic mice. *A–C*, Immunohistochemical study from the 16-week-old AR-97Q/HSP70$^{(tg/-)}$ mice in the spinal anterior horn and skeletal muscle stained with the antibody specific for the HSP70. The immunoreactivity of HSP70 was localized to the nuclei with intense and diffuse staining, and small NIs were present in the anterior horn cell (*A*). A large nuclear inclusion was also present in the anterior horn cell (*B*). Skeletal muscle showed diffuse nuclear staining and NIs (*C*). *D, E*, Western blot analysis of total spinal cord and muscle protein lysate immunolabeled with an antibody against HSP70. AR-97Q/HSP70$^{(tg/-)}$ and AR-97Q/HSP70$^{(tg/tg)}$ mice express higher levels of HSP70 than wild-type (*Wt*) and AR-97Q/HSP70$^{(-/-)}$ mice (*D*). The HSP70 expression level is fivefold higher in AR-97Q/HSP70$^{(tg/-)}$ mice and 10-fold higher in the AR-97Q/HSP70$^{(tg/tg)}$ mice than endogenous HSP70 in AR-97Q/HSP70$^{(-/-)}$ mice in the spinal cord and muscle, respectively (*D*). The AR-97Q transgene expression did not alter HSP70 levels in the spinal cord, whereas the AR-97Q transgene expression gained the respective HSP70 levels in the muscle (*D, E*). Therefore, the AR-97Q transgene expression in the double-transgenics alters HSP70 levels in the muscle but not in the spinal cord. *E*, Western blots of nuclear and cytoplasmic extracts immunolabeled with an antibody against HSP70. HSP70 localized in the nucleus (*N*) as well as in the cytoplasm (*CY*) in the spinal cord and muscle of all lines examined. AR-97Q/HSP70$^{(tg/tg)}$ mice expressed the largest amount of HSP70 in both extracts. *F*, Immunoprecipitation (*IP*) Western blots for HSP70. Soluble fractions were collected from the spinal cord and muscle, and equal protein concentrations were immunoprecipitated with an antibody to the N-terminal portion of AR and immunoblotted for HSP70. Coimmunoprecipitation of the HSP70 chaperone and the polyQ-expanded mutant AR was detected.

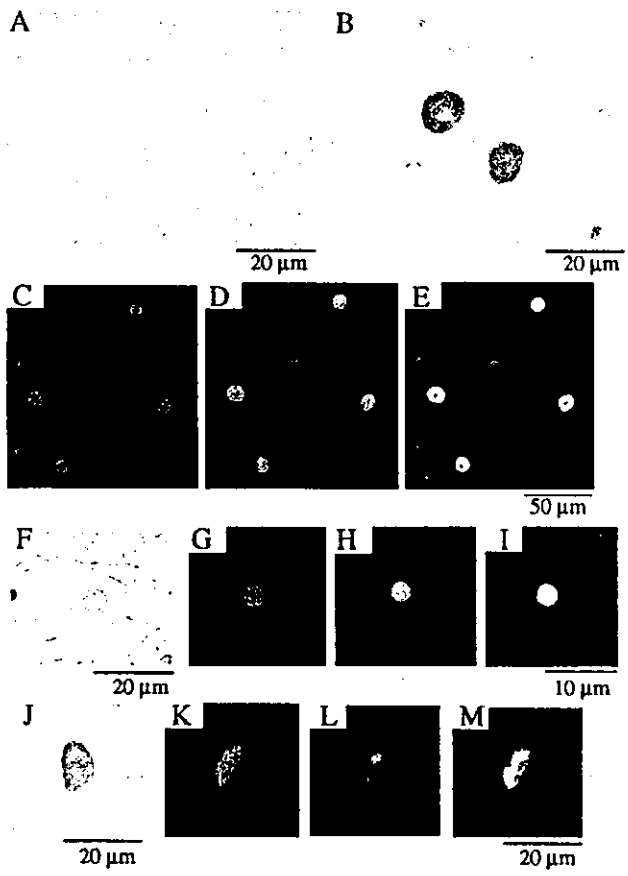

Figure 3. Colocalization of the nuclear-localized HSP70 chaperone with mutant AR. Immunohistochemical analysis for the antibody specific to the HSP70 as well as to the expanded polyQ stretch (immunostained with a monoclonal antibody, 1C2) in the spinal cords of 16-week-old AR-97Q/HSP70$^{(tg/tg)}$ mice (*A–E*) and SBMA patients (*F–M*). Double-labeling immunohistochemistry revealed diffuse nuclear staining for goat anti-HSP70 (*A*) and expanded polyQ (*B*), suggesting that HSP70 and mutant AR are colocalized in the spinal motor neurons of AR-97Q/HSP70$^{(tg/tg)}$ mice. Immunofluorescence double-staining with antibodies against HSP70 and the expanded polyQ also revealed that HSP70 and mutant AR are colocalized as shown in HSP70 (*C, green*), expanded-polyQ (*D, red*), and an overlay of the two signals (*E, yellow*). Diffuse staining of neuronal nuclei for HSP70 is also observed in the spinal neurons (*F, J*) of SBMA patients. Immunofluorescence double-staining with anti-HSP70 (*green*) and anti-expanded polyQ (*red*) antibodies revealed that the HSP70 (*G*) and mutant AR (*H*) are colocalized on the NI (shown in *yellow* in *I*) in the spinal anterior horn cell. The diffuse nuclear colocalization of HSP70 (*K*) and mutant AR (*H*) was also observed in the SBMA posterior horn cell (*M*). This cell also has an NI (*L, M*).

in the AR-97Q/HSP70$^{(tg/-)}$ mice (Fig. 4*B,E*) and much less frequent in the AR-97Q/HSP70$^{(tg/tg)}$ mice (Fig. 4*C,F*). Quantitative assessment of diffuse nuclear staining for 1C2 in the spinal motor neurons (Fig. 4*G*) and muscles (Fig. 4*H*) revealed significantly more positive cells in the AR-97Q/HSP70$^{(-/-)}$ mice than in the AR-97Q/HSP70$^{(tg/-)}$ and AR-97Q/HSP70$^{(tg/tg)}$ mice. However, the 1C2-positive cell populations were not statistically different in the AR-97Q/HSP70$^{(tg/-)}$ and the AR-97Q/HSP70$^{(tg/tg)}$ mice. The neuronal cell population in the spinal ventral horn in the AR-97Q/HSP70$^{(-/-)}$, AR-97Q/HSP70$^{(tg/-)}$, and AR-97Q/HSP70$^{(tg/tg)}$ mice was not significantly decreased compared with that in the wild-type mice (data not shown).

Overexpression of HSP70 decreases the high-molecular-weight mutant AR protein and monomeric mutant AR protein

Western blot analysis showed that the high-molecular-weight form of mutant AR protein complexes was retained in the stacking gel as well as a band of monomeric mutant AR monomer in the spinal cord and muscle of the transgenic mice (Fig. 5). The mutant AR within the stacking gel was diminished in the AR-97Q/HSP70$^{(tg/-)}$ and AR-97Q/HSP70$^{(tg/tg)}$ mice compared with the AR-97Q/HSP70$^{(-/-)}$ mice (Fig. 5*A,B*). In addition, the AR-97Q/HSP70$^{(-/-)}$ mice had more monomeric mutant AR protein than the AR-97Q/HSP70$^{(tg/-)}$ or AR-97Q/HSP70$^{(tg/tg)}$ mice (Fig. 5*A,B*). The mutant AR protein within the stacking gel was found primarily in the nuclear fraction (Fig. 5*C*). The mutant AR within the stacking gel and monomeric form of the nuclear fraction in the spinal cord and muscle were also decreased in the AR-97Q/HSP70$^{(tg/-)}$ and AR-97Q/HSP70$^{(tg/tg)}$ mice (Fig. 5*C*). These observations suggested that the overexpression of HSP70 markedly decreases not only the high-molecular-weight mutant AR protein present primarily in the nuclear fraction but also the monomeric mutant AR protein.

We next performed a filter-trap assay for the quantitative analysis of the large molecular aggregated and soluble monomeric form of the mutant AR protein (Wanker et al., 1999). Only the larger-sized mutant AR protein was retained on the cellulose acetate membrane (pore diameter, 0.2 μm), whereas the nitrocellulose membrane captured proteins of all sizes (Fig. 6*A*). We also put the nitrocellulose membrane under the cellulose acetate membrane to capture the soluble monomeric AR protein passing through this membrane (Fig. 6*B*). Values were normalized to endogenous α-tubulin using the nitrocellulose membrane. Using this approach, we analyzed the ability of the HSP70 to decrease the large aggregated or soluble monomeric mutant AR protein. Overexpression of HSP70 resulted in a significant decrease in large aggregated as well as soluble monomeric mutant AR protein in a dose-dependent manner (Fig. 6*A–C*). The endogenous AR protein was not retained on the cellulose acetate membrane in wild-type mice (data not shown). These results indicate that the HSP70 decreases not only the mutant AR protein complexes in the large aggregated form but also the soluble monomeric mutant AR as observed on Western blot analysis. These observations also suggested that overexpression of HSP70 enhanced the function of the ubiquitin–proteasome pathway and subsequently accelerated the degradation of monomeric mutant AR protein.

Discussion

We generated a transgenic mouse model carrying a full-length AR containing 97 CAGs (Katsuno et al., 2002). This model showed progressive muscular atrophy and weakness as well as diffuse nuclear staining and NIs consisting of the mutant AR. These phenotypes were very pronounced in male transgenic mice, similar to those in SBMA (Katsuno et al., 2002). Here we demonstrate that the overexpression of human HSP70 exerts dose-dependent therapeutic effects on motor dysfunction in this mouse model. Mutant AR and HSP70 colocalized diffusely to the nuclei and to the NIs in the neurons and muscles of the AR-97Q/HSP70 double-transgenic mice. The overexpression of HSP70 served to decrease the nuclear-localized mutant AR protein complexes in large aggregated form in the double-transgenic mice. Monomeric mutant AR was also significantly reduced by HSP70 overexpression, suggesting that it could accelerate the turnover of mutant AR.

In our SBMA transgenic mouse model, nuclear translocation of mutant AR, which is dependent on the testosterone level, has been demonstrated to be essential for mutant AR-induced neurotoxicity (Katsuno et al., 2002). Reduction of the testosterone level by castration diminished nuclear-localized mutant AR and markedly prevented phenotypic expression in the male trans-

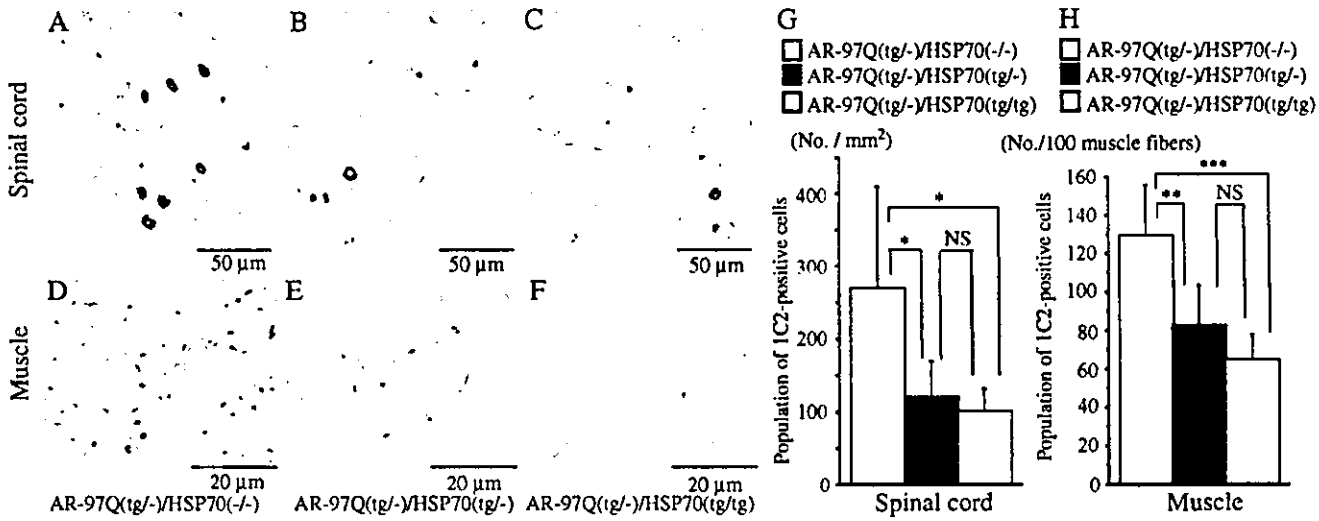

Figure 4. HSP70 decreases nuclear-localized mutant AR in double-transgenic mice. Immunohistochemical study of the spinal anterior horn (*A–C*) and muscle (*D–F*) of AR-97Q/HSP70$^{(-/-)}$ and AR-97Q/HSP70 double-transgenic mice stained with a monoclonal antibody (1C2) against abnormally expanded polyQ (16 weeks old). AR-97Q/HSP70$^{(-/-)}$ mice have intense and frequent staining for 1C2 in the nucleus (*A, D*). AR-97Q/HSP70$^{(tg/-)}$ (*B, E*), and AR-97Q/HSP70$^{(tg/tg)}$ (*C, F*) mice exhibit low levels of 1C2 staining in the nucleus. *G, H*, Quantitative assessment of diffuse nuclear staining for 1C2 in the spinal ventral horn (*G*) and muscle (*H*). Positively stained nuclei were estimated by counting in the thoracic spinal ventral horn and muscle using six transgenic mice (16 weeks of age). There are significantly more 1C2-positive cells in AR-97Q/HSP70$^{(-/-)}$ mice than in AR-97Q/HSP70$^{(tg/-)}$ mice or AR-97Q/HSP70$^{(tg/tg)}$ mice in both tissues. Results are expressed as means ± SD for six mice. The differences in 1C2-positive cell populations are not statistically significant between AR-97Q/HSP70$^{(tg/-)}$ and AR-97Q/HSP70$^{(tg/tg)}$ mice. $^{*}p < 0.05$; $^{**}p < 0.01$; $^{***}p < 0.001$.

genic mice, whereas testosterone administration enhanced the nuclear localization of mutant AR and caused significant motor dysfunction in the female transgenic mice (Katsuno et al., 2002). In particular, the large aggregated complexes of the mutant AR protein detected in the stacking gel or slowly migrating species in the Western blot analysis in the nuclear fraction were well correlated with the phenotypic expression in this mouse model (Katsuno et al., 2002). This suggested that oligomeric or polymeric mutant AR large complex molecules positively associated with other molecules would exert the toxicity rather than monomeric mutant AR (Katsuno et al., 2002).

In the present study, we demonstrated that the amount of nuclear-localized mutant AR protein, particularly that of the large complex form present in the stacking gel or trapped by the cellulose acetate membrane, was significantly reduced in the AR-97/HSP70 double-transgenic mice. Thus, the overexpression of HSP70 is suggested to exert its amelioration of the phenotypic expression by diminishing the amount of nuclear-localized mutant AR protein. However, in the previously reported SCA1 transgenic mouse model, NIs of the mutant protein were not apparently decreased in the double-transgenic mice with rat HSP70 overexpression, although the neurological deficit and neuronal degeneration were ameliorated (Cummings et al., 2001). Because the gain of amelioration for phenotypic expression in the model mice of Cummings et al. (2001) was mild even in the double-transgenics with HSP70 homozygotes, the change in the frequency of the NIs would not have been significant enough to detect. In our mouse model, NIs were present only in the small subpopulation of neurons and muscles, particularly in the early phase of phenotypic expression, whereas the 1C2-positive nuclei were abundant (Katsuno et al., 2002). In addition, 1C2-positive neurons are more extensive than those of NI-bearing neurons in the tissues of the autopsied samples from patients with polyQ diseases, and the distribution of 1C2-positive neurons is well correlated with the neurological symptoms (Yamada et al., 2001). These observations suggest that 1C2 staining is a more sensitive histological marker for the detection of the nuclear localization of the mutant protein with an expanded polyQ stretch compared with NIs detected by antibodies for the responsible protein.

The interesting observation in our study was the diminution of monomeric mutant AR in the double-transgenic mice with overexpression of HSP70. Recently, HSP70 overexpression in the cell culture model has revealed enhanced solubility of mutant AR with an expanded polyQ and degradation through the ubiquitin–proteasome system (Bailey et al., 2002). Overexpression of chaperones generally enhances the function of the ubiquitin–proteasome pathway and subsequently accelerates protein degradation (Bukau and Horwich, 1998). The ubiquitin–proteasome pathway, particularly its activity, is known to be related to chaperone expression levels (Bukau and Horwich, 1998). The molecular mechanism for this relationship remains unsolved, but recently CHIP (C terminal of HSC70-interacting protein), U-box-type E3 ubiquitin ligase, has been shown to interact with HSP90 or HSP70 (Connel et al., 2001) and ubiquitylate unfolded proteins trapped by molecular chaperones and degrades them, thus acting as a "quality control E3" (Murata et al., 2001). Furthermore, there is a cofactor of HSC70/HSP70, Bcl-2 associated athanogene 1, which possesses a ubiquitin-like domain and promotes binding of HSC70/HSP70 to the proteolytic complex (Lüders et al., 2000). Although such coupling factors between the HSP70 chaperone system and the protein degradation machinery for mutant AR are unknown at present, if the similar E3 for mutant AR is present, it could ubiquitylate and degrade mutant AR as a result of interacting with HSP70. In this scenario, the overexpression of HSP70 may accelerate E3-dependent capture of mutant AR and its degradation through the proteasome pathway. A remarkable reduction of the monomeric mutant AR in the double-transgenics with HSP70 overexpression can be the reflection of the accelerated degradation of mutant AR through the HSP70-mediated E3–proteasome system. Interaction between mutant AR and HSP70 detected by coimmunoprecipitation and Western blot analysis in the double-transgenic mice would support this view. The overexpression of HSP70 could enhance the degradation of the mo-

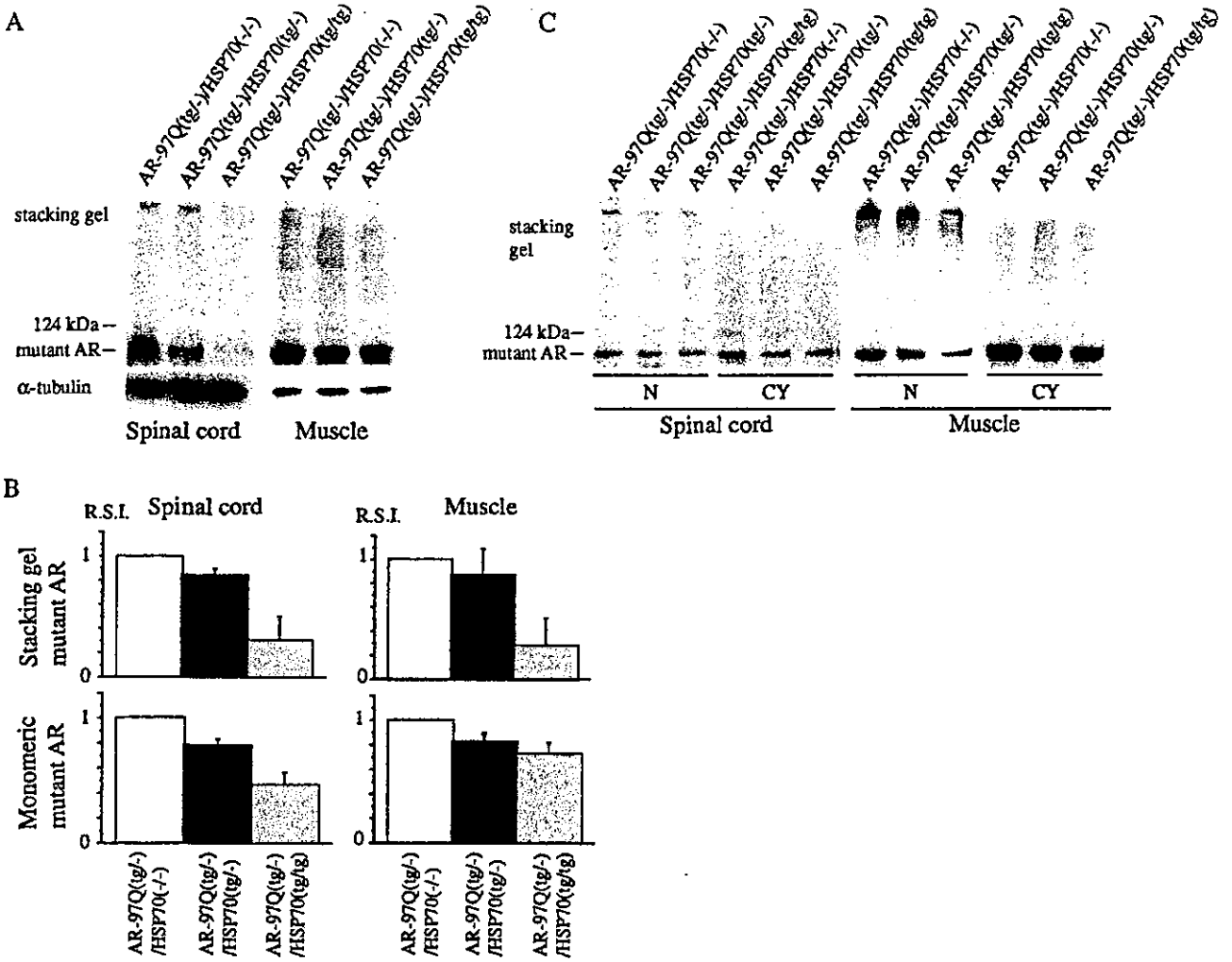

Figure 5. HSP70 decreases nuclear-localized mutant AR protein complexes as well as monomeric mutant AR. *A*, *B*, Western blot analysis of total tissue homogenates from the spinal cord and muscle of AR-97Q/HSP70$^{(-/-)}$, AR-97Q/HSP70$^{(tg/-)}$, and AR-97Q/HSP70$^{(tg/tg)}$ mice (16 weeks of age) immunolabeled by an antibody against AR (N-20). The mutant AR appearing within the stacking gel and monomeric mutant AR were diminished in AR-97Q/HSP70$^{(tg/-)}$ and AR-97Q/HSP70$^{(tg/tg)}$ mice compared with AR-97Q/HSP70$^{(-/-)}$ mice (*A*, *B*). Values of mutant AR were normalized to endogenous α-tubulin and expressed as the ratio to those of AR-97Q/HSP70$^{(-/-)}$ mice (*B*). Values are expressed as means ± SD for three mice. *C*, Western blot analysis of nuclear (*N*) and cytoplasmic (*CY*) fractions from the spinal cord and muscle of AR-97Q/HSP70$^{(-/-)}$, AR-97Q/HSP70$^{(tg/-)}$, and AR-97Q/HSP70$^{(tg/tg)}$ mice (16 weeks of age) immunolabeled by N-20. Mutant AR protein within the stacking gel was found primarily in the nuclear fraction. The mutant AR within the stacking gel of the nuclear fraction also significantly decreased in the spinal cord and muscle of AR-97Q/HSP70$^{(tg/tg)}$ mice. *R.S.I.*, Relative signal intensity.

nomeric mutant AR, presumably through the HSP70-interacting quality control E3 activation, and subsequently it could reduce the amount of nuclear-localized mutant AR, resulting in the amelioration of phenotypic expression induced by mutant AR. To substantiate this, however, one needs to identify the HSP70-interacting E3 ligase, which recognizes mutant AR as a substrate.

Another possibility is that overexpressed HSP70 directly renaturates the misfolded mutant AR and normalizes the interaction of mutant AR with proteins that are essential to maintain the cell function (Hendricks and Hartl, 1993). The overexpression of HSP70 and HSP40 or HSC70 and *Drosophila* human DNAJ homolog-1 (dHdj-1) changed the distribution and morphologic pattern of NI formation of mutant huntingtin and ataxin-1 (Cummings et al., 1998; Fernandez-Funez et al., 2000; Muchowski et al., 2000). The overexpression of dHdj-1 and HSP70 increased the proportion of the monomeric mutant protein with an expanded polyQ, suggesting that chaperones modulate the biochemical properties of mutant polyQ-bearing protein (Chan et al., 2000). It has been proposed that the disease proteins with an expanded polyQ participate in inappropriate protein–protein interactions that lead to cell dysfunction and eventual cell death (Sherman and Goldberg, 2001). Molecular chaperones can be involved in the conformational modification by stabilizing the unfolded mutant proteins and can facilitate or inhibit the interaction with self or other proteins (Opal and Zoghbi, 2002). To date, a number of proteins that interact with polyQ-bearing disease protein have been cloned, including huntingtin-associated protein (Li et al., 1995), huntingtin-interacting protein (Kalchman et al., 1997), glyceraldehyde-3-phosphate dehydrogenase (Burke et al., 1996), leucine-rich acidic nuclear protein (Matilla et al., 1997), polyglutamine tract-binding protein-1 (Waragai et al., 1999), 130 kDa human TATA-binding protein-associated factor subunit of the human transcription factor TFIID (Shimohata et al., 2000), and cAMP response element-binding protein (CREB) binding protein (CBP) (Nucifora et al., 2001; Zander et al., 2001). CBP has been demonstrated to interact with mutant AR, colocalize in the NIs, and reduce the mutant AR-induced cell toxicity by CBP overexpression in the cell culture model by modifying CBP-dependent transcriptional activity (McCampbell et al., 2000). HSP70 may reduce the toxicity of

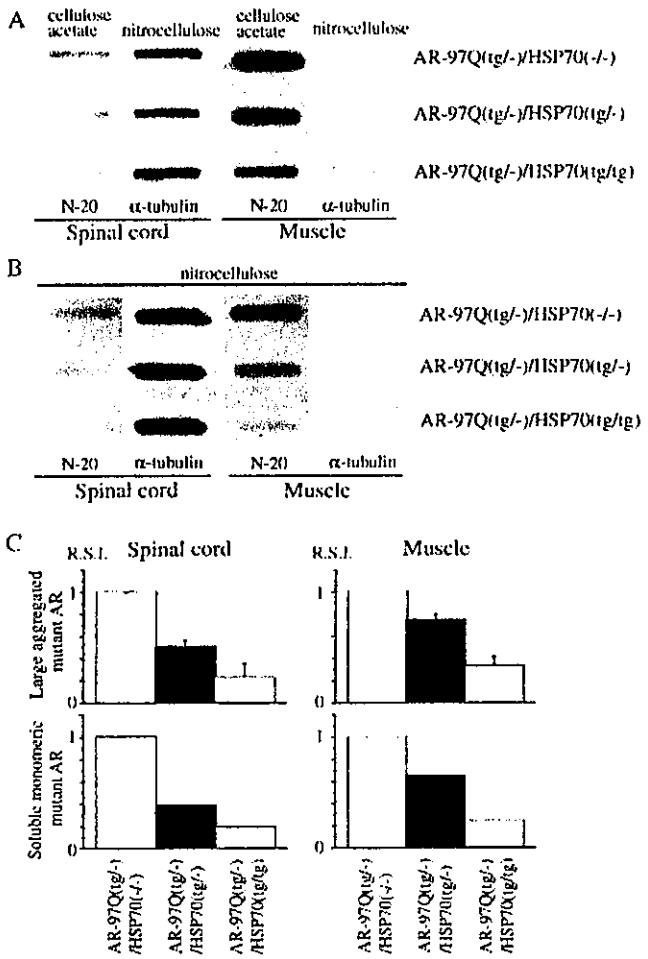

Figure 6. HSP70 decreases large aggregated mutant AR protein and soluble monomeric mutant AR protein. *A–C*, Filter-trap assay of total tissue homogenates from the spinal cord and muscle of AR-97Q/HSP70$^{(-/-)}$, AR-97Q/HSP70$^{(tg/-)}$, and AR-97Q/HSP70$^{(tg/tg)}$ mice (16 weeks of age) immunolabeled by an antibody against AR (N-20). Large aggregated mutant AR complexes were trapped by the cellulose acetate membrane (*A*), and soluble monomeric mutant AR passing through the cellulose acetate membrane was trapped by the nitrocellulose membrane beneath the cellulose acetate membrane (*B*). Endogenous α-tubulin using the nitrocellulose membrane was also shown (*A*, *B*). The normalized value of large aggregated mutant AR and soluble monomeric mutant AR against endogenous α-tubulin is shown in *C*. Relative values against those of AR-97Q/HSP70$^{(-/-)}$ mice were expressed as means ± SD for three mice or a mean of two mice (*C*). The trapped AR protein was reduced in the spinal cord and muscle of AR-97Q/HSP70$^{(tg/-)}$ and AR-97Q/HSP70$^{(tg/tg)}$ mice in both membranes (*A*, *B*). This reduction was most evident in AR-97Q/HSP70$^{(tg/tg)}$ mice (*A–C*), suggesting that the overexpression of HSP70 resulted in a significant, dose-dependent decrease in large aggregated and soluble monomeric mutant AR protein. *R.S.I.*, Relative signal intensity.

mutant AR proteins through the inhibition or acceleration of the interaction with these proteins. However, interacting protein involvement in association with mutant AR still needs to be investigated.

The other possible avenue by which HSP70 acts to improve polyQ-induced toxicity is the anti-apoptotic activities of HSP70. HSP70 suppresses apoptosis by inhibiting the *c*-Jun N-terminal kinase (Gabai et al., 1998) or by inhibiting cytochrome *c* release and caspase-3 activation (Li et al., 2000; Jana et al., 2001). Furthermore, HSP40 and mammalian relative of DNAJ chaperones can inhibit caspase-3 and caspase-9 activation mediated by mutant huntingtin, independent of huntingtin aggregation (Zhou et al., 2001; Chuang et al., 2002). However, the involvement of anti-apoptotic activities of HSPs in protection against mutant AR toxicity through reducing the nuclear-localized mutant AR remains to be elucidated.

In summary, the overexpression of HSP70 significantly ameliorates the phenotypes of SBMA transgenic mice by reducing the amount of nuclear-localized mutant AR protein, particularly that of the large complex form. The amount of monomeric mutant AR was also reduced by HSP70 overexpression, suggesting enhanced degradation of mutant AR. A recent study revealed that the ansamycin antibiotic Geldanamycin induced a heat shock response and inhibited aggregation of mutant huntingtin in COS-1 cells (Sittler et al., 2001). Thus, HSP70 overexpression would provide a potential therapeutic avenue for SBMA and other polyQ diseases.

References

Adachi H, Kume A, Li M, Nakagomi Y, Niwa H, Do J, Sang C, Kobayashi Y, Doyu M, Sobue G (2001) Transgenic mice with an expanded CAG repeat controlled by the human AR promoter show polyglutamine nuclear inclusions and neuronal dysfunction without neuronal cell death. Hum Mol Genet 10:1039–1048.

Bailey CK, Andriola IF, Kampinga HH, Merry DE (2002) Molecular chaperones enhance the degradation of expanded polyglutamine repeat androgen receptor in a cellular model of spinal and bulbar muscular atrophy. Hum Mol Genet 11:515–523.

Bukau KT, Horwich AL (1998) The Hsp70 and Hsp60 chaperone machines. Cell 92:351–366.

Burke JR, Enghild JJ, Martin ME, Jou YS, Myers RM, Roses AD, Vance JM, Strittmatter WJ (1996) Huntingtin and DRPLA proteins selectively interact with the enzyme GAPDH. Nat Med 2:347–350.

Carmichael J, Chatellier J, Woolfson A, Milstein C, Fersht AR, Rubinsztein DC (2000) Bacterial and yeast chaperones reduce both aggregate formation and cell death in mammalian cell models of Huntington's disease. Proc Natl Acad Sci USA 97:9701–9705.

Chai Y, Koppenhafer SL, Bonini NM, Paulson HL (1999) Analysis of the role of heat shock protein (Hsp) molecular chaperones in polyglutamine disease. J Neurosci 19:10338–10347.

Chan HYE, Warrick JM, Gray-Board GL, Paulson HL, Bonini NM (2000) Mechanisms of chaperone suppression of polyglutamine disease: selectivity, synergy and modulation of protein solubility in *Drosophila*. Hum Mol Genet 9:2811–2820.

Chuang JZ, Zhou H, Zhu M, Li SH, Li XJ, Sung CH (2002) Characterization of a brain-enriched chaperone, MRJ, that inhibits Huntingtin aggregation and toxicity independently. J Biol Chem 277:19831–19838.

Connel P, Ballinger CA, Jiang J, Wu Y, Thompson LJ, Höfeld J, Patterson C (2001) The co-chaperone CHIP regulates protein triage decisions mediated by heat shock proteins. Nat Cell Biol 3:93–96.

Cummings CJ, Mancini MA, Antalffy B, DeFranco DB, Orr HT, Zoghbi HY (1998) Chaperone suppression of aggregation and altered subcellular proteasome localization imply protein misfolding in SCA1. Nat Genet 19:148–154.

Cummings CJ, Sun Y, Opal P, Antalffy B, Mestril R, Orr HT, Dillmann WH, Zoghbi HY (2001) Overexpression of inducible HSP70 chaperone suppresses neuropathology and improves motor function in SCA1 mice. Hum Mol Genet 10:1511–1518.

Doyu M, Sobue G, Mukai E, Kachi T, Yasuda T, Mitsuma T, Takahashi A (1992) Severity of X-linked recessive bulbospinal neuronopathy correlates with size of the tandem CAG repeat in androgen receptor gene. Ann Neurol 23:707–710.

Fernandez-Funez P, Nino-Rosales ML, de Gouyon B, She WC, Luchak JM, Martinez P, Turiegano E, Benito J, Capovilla M, Skinner PJ, McCall A, Canal I, Orr HT, Zoghbi HY, Botas J (2000) Identification of genes that modify ataxin-1-induced neurodegeneration. Nature 408:101–106.

Gabai VL, Meriin AB, Yaglom JA, Volloch VZ, Sherman MY (1998) Role of Hsp70 in regulation of stress-kinase JNK: implications in apoptosis and aging. FEBS Lett 438:1–4.

Hendricks JP, Hartl FU (1993) Molecular chaperone functions of heat-shock proteins. Annu Rev Biochem 62:349–384.

Huynh DP, Figueroa K, Hoang N, Pulst SM (2000) Nuclear localization or inclusion body formation of ataxin-2 are not necessary for SCA2 pathogenesis in mouse or human. Nat Genet 26:44–50.

Igarashi S, Tanno Y, Onodera O, Yamazaki M, Sato S, Ishikawa A, Miyatani N, Nagashima M, Ishikawa Y, Sahashi K, Ibi T, Miyatake T, Tsuji S (1992)

Strong correlation between the number of CAG repeats in androgen receptor genes and the clinical onset of features of spinal and bulbar muscular atrophy. Neurology 42:2300–2302.

Jana NR, Tanaka M, Wang GH, Nukina N (2000) Polyglutamine length-dependent interaction of Hsp40 and Hsp70 family chaperones with truncated N-terminal huntingtin: their role in suppression of aggregation and cellular toxicity. Hum Mol Genet 9:2009–2018.

Jana NR, Zemskov EA, Wang GH, Nukina N (2001) Altered proteasomal function due to the expression of polyglutamine-expanded truncated N-terminal huntingtin induces apoptosis by caspase activation through mitochondrial cytochrome c release. Hum Mol Genet 10:1049–1059.

Kalchman MA, Koide HB, McCutcheon K, Graham RK, Nichol K, Nishiyama K, Kazemi-Esfarjani P, Lynn FC, Wellington C, Metzler M, Goldberg YP, Kanazawa I, Gietz RD, Hayden MR (1997) HIP1, a human homologue of *S. cerevisiae* Sla2p, interacts with membrane-associated huntingtin in the brain. Nat Genet 16:44–53.

Katsuno M, Adachi H, Kume A, Li M, Nakagomi Y, Niwa H, Sang C, Kobayashi Y, Doyu M, Sobue G (2002) Testosterone reduction prevents phenotypic expression in a transgenic mouse model of spinal and bulbar muscular atrophy. Neuron 35:843–854.

Kennedy WR, Alter M, Sung JH (1968) Progressive proximal spinal and bulbar muscular atrophy of late onset: a sex-linked recessive trait. Neurology 18:671–680.

Kobayashi Y, Sobue G (2001) Protective effect of chaperones on polyglutamine diseases. Brain Res Bull 56:165–168.

Kobayashi Y, Kume A, Li M, Doyu M, Hata M, Ohtsuka K, Sobue G (2000) Chaperones Hsp70 and Hsp40 suppress aggregate formation and apoptosis in cultured neuronal cells expressing truncated androgen receptor protein with expanded polyglutamine tract. J Biol Chem 275:8772–8778.

La Spada AR, Roling DB, Harding AE, Warner CL, Spiegel R, Hausmanowa-Petrusewicz I, Yee WC, Fischbeck KH (1992) Meiotic stability and genotype-phenotype correlation of the trinucleotide repeat in X-linked spinal and bulbar muscular atrophy. Nat Genet 2:301–304.

Li CY, Lee JS, Ko YG, Kim JI, Seo JS (2000) Heat shock protein 70 inhibits apoptosis downstream of cytochrome c release and upstream of caspase-3 activation. J Biol Chem 275:25665–25671.

Li M, Miwa S, Kobayashi Y, Merry DE, Tanaka F, Doyu M, Hashizume Y, Fischbeck KH, Sobue G (1998a) Nuclear inclusions of the androgen receptor protein in spinal and bulbar muscular atrophy. Ann Neurol 44:249–254.

Li M, Nakagomi Y, Kobayashi Y, Merry DE, Tanaka F, Doyu M, Mitsuma T, Fischbeck KH, Sobue G (1998b) Nonneural nuclear inclusions of androgen receptor protein in spinal and bulbar muscular atrophy. Am J Pathol 153:695–701.

Li XJ, Li SH, Sharp AH, Nucifora Jr FC, Schilling G, Lanahan A, Worley P, Snyder SH, Ross CA (1995) A huntingtin-associated protein enriched in brain with implications for pathology. Nature 378:398–402.

Lüders J, Demand J, Höhfeld J (2000) The ubiquitin-related BAG-1 provides a link between the molecular chaperones Hsc70/Hsp70 and the proteasome. J Biol Chem 275:4613–4617.

Matilla A, Koshy BT, Cummings CJ, Isobe T, Orr HT, Zoghbi HY (1997) The cerebellar leucine-rich acidic nuclear protein interacts with ataxin-1. Nature 389:974–978.

McCampbell A, Taylor JP, Taye AA, Robitschek J, Li M, Walcott J, Merry D, Chai Y, Paulson H, Sobue G, Fischbeck KH (2000) CREB-binding protein sequestration by expanded polyglutamine. Hum Mol Genet 9:2197–2202.

Muchowski PJ, Schaffar G, Sittler A, Wanker EE, Hayer-Hartl MK, Hartl FU (2000) Hsp70 and hsp40 chaperones can inhibit self-assembly of polyglutamine proteins into amyloid-like fibrils. Proc Natl Acad Sci USA 97:7841–7846.

Murata S, Minami Y, Minami M, Chiba T, Tanaka K (2001) CHIP is a chaperone-dependent E3 ligase that ubiquitylates unfolded protein. EMBO Rep 2:1133–1138.

Nucifora Jr FC, Sasaki M, Peters MF, Huang H, Cooper JK, Yamada M, Takahashi H, Tsuji S, Troncoso J, Dawson VL, Dawson TM, Ross CA (2001) Interference by huntingtin and atrophin-1 with cbp-mediated transcription leading to cellular toxicity. Science 291:2423–2428.

Opal P, Zoghbi HY (2002) The role of chaperones in polyglutamine disease. Trends Mol Med 8:232–236.

Plumier JC, Ross BM, Currie RW, Angelidis CE, Kaziaris H, Kollias G, Pagoulatos GN (1995) Transgenic mice expressing the human heat shock protein 70 have improved post-ischemic myocardial recovery. J Clin Invest 95:1854–1860.

Ross CA (2002) Polyglutamine pathogenesis: emergence of unifying mechanisms for Huntington's disease and related disorders. Neuron 35:819–822.

Schmidt T, Lindenberg KS, Krebs A, Schols L, Laccone F, Herms J, Rechsteiner M, Riess O, Landwehrmeyer GB (2002) Protein surveillance machinery in brains with spinocerebellar ataxia type 3: redistribution and differential recruitment of 26S proteasome subunits and chaperones to neuronal intranuclear inclusions. Ann Neurol 51:302–310.

Sherman MY, Goldberg AL (2001) Cellular defenses against unfolded proteins: a cell biologist thinks about neurodegenerative diseases. Neuron 29:15–32.

Shimohata T, Nakajima T, Yamada M, Uchida C, Onodera O, Naruse S, Kimura T, Koide R, Nozaki K, Sano Y, Ishiguro H, Sakoe K, Ooshima T, Sato A, Ikeuchi T, Oyake M, Sato T, Aoyagi Y, Hozumi I, Nagatsu T, et al. (2000) Expanded polyglutamine stretches interact with TAFII130,interfering with CREB-dependent transcription. Nat Genet 26:29–36.

Sittler A, Lurz R, Lueder G, Priller J, Hayer-Hartl MK, Hartl FU, Lehrach H, Wanker EE (2001) Geldanamycin activates a heat shock response and inhibits huntingtin aggregation in a cell culture model of Huntington's disease. Hum Mol Genet 10:1307–1315.

Sobue G, Hashizume Y, Mukai E, Hirayama M, Mitsuma T, Takahashi A (1989) X-linked recessive bulbospinal neuronopathy: a clinicopathological study. Brain 112:209–232.

Stenoien DL, Cummings CJ, Adams HP, Mancini MG, Patel K, DeMartino GN, Marcelli M, Weigel NL, Mancini MA (1999) Polyglutamine-expanded androgen receptors form aggregates that sequester heat shock proteins,proteasome components and SRC-1,and are suppressed by the HDJ-2 chaperone. Hum Mol Genet 8:731–741.

Takahashi A (2001) Hiroshi Kawahara (1858–1918). J Neurol 248:241–242.

Tanaka F, Doyu M, Ito Y, Matsumoto M, Mitsuma T, Abe K, Aoki M, Itoyama Y, Fischbeck KH, Sobue G (1996) Founder effect in spinal and bulbar muscular atrophy (SBMA). Hum Mol Genet 5:1253–1257.

Tanaka F, Reeves MF, Ito Y, Matsumoto M, Li M, Miwa S, Inukai A, Yamamoto M, Doyu M, Yoshida M, Hashizume Y, Terao S, Mitsuma T, Sobue G (1999) Tissue-specific somatic mosaicism in spinal and bulbar muscular atrophy (SBMA) is dependent on CAG repeat length and androgen receptor gene expression level. Am J Hum Genet 65:966–973.

Terao S, Sobue G, Hashizume Y, Li M, Inagaki T, Mitsuma T (1996) Age-related changes in human spinal ventral horn cells with special reference to the loss of small neurons in the intermediate zone: a quantitative analysis. Acta Neuropathol (Berl) 92:109–114.

Waelter S, Boeddrich A, Lurz R, Scherzinger E, Lueder G, Lehrach H, Wanker EE (2001) Accumulation of mutant huntingtin fragments in aggresome-like inclusion bodies as a result of insufficient protein degradation. Mol Biol Cell 12:1393–1407.

Wanker EE, Scherzinger E, Heiser V, Sittler A, Eickhoff H, Lehrach H (1999) Membrane filter assay for detection of amyloid-like polyglutamine-containing protein aggregates. Methods Enzymol 309:375–386.

Waragai M, Lammers C, Takeuchi S, Imafuku I, Udagawa Y, Kanazawa I, Kawabata M, Mouradian MM, Okazawa H (1999) PQBP-1,a novel polyglutamine tract-binding protein,inhibits transcription activation by Brn-2 and affects cell survival. Hum Mol Genet 8:977–987.

Warrick JM, Chan HY, Gray-Board GL, Chai Y, Paulson HL, Bonini NM (1999) Suppression of polyglutamine-mediated neurodegeneration in *Drosophila* by the molecular chaperone HSP70. Nat Genet 23:425–428.

Yamada M, Wood JD, Shimohata T, Hayashi S, Tsuji S, Ross CA, Takahashi H (2001) Widespread occurrence of intranuclear atrophin-1 accumulation in the central nervous system neurons of patients with dentatorubral-pallidoluysian atrophy. Ann Neurol 49:14–23.

Zander C, Takahashi J, Hachimi KHE, Fujigasaki H, Albanese V, Lebre AS, Stevanin G, Duyckaerts C, Brice A (2001) Similarities between spinocerebellar ataxia type 7 (SCA7) cell models and human brain: proteins recruited in inclusions and activation of caspase-3. Hum Mol Genet 10:2569–2579.

Zhou H, Li SH, Li XJ (2001) Chaperone suppression of cellular toxicity of huntingtin is independent of polyglutamine aggregation. J Biol Chem 276:48417–48424.

Zoghbi HY, Orr HT (2000) Glutamine repeats and neurodegeneration. Annu Rev Neurosci 23:217–247.

THE JOURNAL OF BIOLOGICAL CHEMISTRY
Vol. 278, No. 27, Issue of July 4, pp. 25143–25150, 2003
Printed in U.S.A.

Hsp105α Suppresses the Aggregation of Truncated Androgen Receptor with Expanded CAG Repeats and Cell Toxicity*

Received for publication, March 24, 2003, and in revised form, April 21, 2003
Published, JBC Papers in Press, April 24, 2003, DOI 10.1074/jbc.M302975200

Keiichi Ishihara‡, Nobuyuki Yamagishi‡, Youhei Saito‡, Hiroaki Adachi§, Yasushi Kobayashi§, Gen Sobue§, Kenzo Ohtsuka¶, and Takumi Hatayama‡‖

From the ‡Department of Biochemistry, Kyoto Pharmaceutical University, 5 Nakauchi-cho, Misasagi, Yamashina-ku, Kyoto 607-8414, the §Department of Neurology, Nagoya University Graduate School of Medicine, 65 Tsurumai-cho Showa-ku, Nagoya 466-8550, and the ¶Department of Environmental Biology, College of Bioscience and Biotechnology, Chubu University, Matsumoto-cho 1200, Kasugai 487-8501, Japan

Spinal and bulbar muscular atrophy (SBMA) is a neurodegenerative disorder caused by the expansion of a polyglutamine tract in the androgen receptor (AR). The N-terminal fragment of AR containing the expanded polyglutamine tract aggregates in cytoplasm and/or in nucleus and induces cell death. Some chaperones such as Hsp40 and Hsp70 have been identified as important regulators of polyglutamine aggregation and/or cell death in neuronal cells. Recently, Hsp105α, expressed at especially high levels in mammalian brain, has been shown to suppress apoptosis in neuronal cells and prevent the aggregation of protein caused by heat shock *in vitro*. However, its role in polyglutamine-mediated cell death and toxicity has not been studied. In the present study, we examined the effects of Hsp105α on the aggregation and cell toxicity caused by expansion of the polyglutamine tract using a cellular model of SBMA. The transient expression of truncated ARs (tARs) containing an expanded polyglutamine tract caused aggregates to form in COS-7 and SK-N-SH cells and concomitantly apoptosis in the cells with the nuclear aggregates. When Hsp105α was overexpressed with tAR97 in the cells, Hsp105α was colocalized to aggregates of tAR97, and the aggregation and cell toxicity caused by expansion of the polyglutamine tract were markedly reduced. Both β-sheet and α-helix domains, but not the ATPase domain, of Hsp105α were necessary to suppress the formation of aggregates *in vivo* and *in vitro*. Furthermore, Hsp105α was found to localize in nuclear inclusions formed by ARs containing an expanded polyglutamine tract in tissues of patients and transgenic mice with SBMA. These findings suggest that overexpression of Hsp105α suppresses cell death caused by expansion of the polyglutamine tract without chaperone activity, and the enhanced expression of the essential domains of Hsp105α in brain may provide an effective therapeutic approach for CAG repeat diseases.

Spinal and bulbar muscular atrophy (SBMA)[1] is an X-linked motor neuropathy characterized by proximal muscle atrophy, weakness, contraction fasciculation, and bulbar involvement (1, 2). In SBMA patients, a normally polymorphic CAG repeat (10–36 CAGs) in exon 1 of the androgen receptor (AR) gene expands to 40–62 CAGs (3), and nuclear inclusions containing mutant and truncated ARs with an expanded polyglutamine tract are characteristically found in the residual motor neurons in the brain stem and spinal cord (4) as well as in the skin, testis, and other visceral organs (5). In addition to SBMA, expansions of CAG repeats encoding polyglutamine tracts in unrelated proteins are responsible for at least another eight different neurodegenerative diseases including Huntington's disease (6), dentatorubral pallidoluysian atrophy (7, 8), Machado-Joseph disease (9), and several types of spinocerebellar ataxia (10–15). All of these disorders show a late onset of neurological symptoms with progressive neuronal dysfunction and eventual neuronal loss, although the susceptible regions in the nervous system differ among the various disorders. The appearance of intranuclear aggregates/inclusions in neurons is associated with these neurodegenerative diseases. The intranuclear inclusions contain the insoluble protein aggregates of abnormal proteins or their fragments, heat shock proteins, and components of the ubiquitin-dependent proteasome degradation pathway (16, 17). Although the nature of the toxic insult of a polyglutamine mutation and its cell-biological consequences in each disease are unclear, it is possible that the polyglutamine expansion interferes with basic cellular processes such as transcription, protein degradation, and survival/death signaling (17). However, the exact role of these protein aggregates in polyglutamine pathology is still controversial because large polyglutamine aggregates may provide an advantage over small oligomers by exposing less potentially dangerous protein surfaces (18). The cellular components involved in protein folding and degradation are also associated with intracellular inclusions in other neurodegenerative diseases not caused by polyglutamine expansion, including Alzheimer's, Parkinson's, and the prion diseases (19), which suggests that common mechanistic principles may underlie these misfolding diseases in general.

A considerable effort has been made to find molecules that suppress polyglutamine aggregation and cell death/toxicity for therapeutic purposes (20–22). In general, the misfolding and aggregation of proteins are prevented by molecular chaperones (23, 24). Some molecular chaperones such as heat shock protein (Hsp) 70 and Hsp40 have recently been identified as important regulators of polyglutamine aggregation and/or cell death in *in*

* This work was supported in part by a grant-in-aid for scientific research from the Ministry of Education, Science, Culture, and Sports of Japan (to T. H.). The costs of publication of this article were defrayed in part by the payment of page charges. This article must therefore be hereby marked "*advertisement*" in accordance with 18 U.S.C. Section 1734 solely to indicate this fact.

‖ To whom correspondence should be addressed. Fax: 81-75-595-4758; E-mail: hatayama@mb.kyoto-phu.ac.jp.

[1] The abbreviations used are: SBMA, spinal and bulbar muscular atrophy; AR, androgen receptor; BSA, bovine serum albumin; GFP, green fluorescent protein; HA, hemagglutinin; PBS, phosphate-buffered saline; tAR, truncated androgen receptor; TUNEL, terminal nucleotidyl transferase-mediated UTP nick end labeling.

TABLE I
Primers used for construction of expression plasmids for Hsp105α deletion mutants

Expression in mammallan cell
Hsp105N1 (a.a. 1–392)
Sense: 5′-CGGAGAAAGAATTGCACACTG-3′
Antisense: 5′-TCTAGAGGGCCCTTCGAACAA-3′
Hsp105N2 (a.a. 1–511)
Sense: 5′-GGGGTACCCAGCCATGTCGGTGGTT-3′
Antisense: 5′-TCTAGAGGGCCCTTCGAACAA-3′
Hsp105N3 (a.a. 1–606)
Sense: 5′-TAACTGCCATACCAAGTTGGC-3′
Antisense: 5′-TCTAGAGGGCCCTTCGAACAA-3′
Hsp105C1 (a.a. 605–858)
Sense: 5′-GGGGATCCACCATGCTCGAGGCAGACATGGAATGT-3′
Antisense: 5′-GCTCTAGACCTAGTCCAGGTCCATGTTGAC-3′
Hsp105C2 (a.a. 511–858)
Sense: 5′-GGGGATCCACCATGCTCGAGGCAGACATGGAATGT-3′
Antisense: 5′-GCTCTAGACCTAGTCCAGGTCCATGTTGAC-3′
Hsp105C3 (a.a. 386–858)
Sense: 5′-GGGGATCCACCATGCCGGCATTTAAAGTTAGAGAG-3′
Antisense: 5′-GCTCTAGACCTAGTCCAGGTCCATGTTGAC-3′
Hsp105Δβ (a.a. 1–392 + a.a. 551–858)
Sense: 5′-CTCGAGGCAGACATGGAATGTCCA-3′
Antisense: 5′-AGAAAGAATTGCACACTGCAGTGCAC-3′
Hsp105ΔβL (a.a. 1–392 + a.a. 605–858)
Sense: 5′-GGGAGAGACCTTCTTAACATGTATATTG-3′
Antisense: 5′-AGAAAGAATTGCACACTGCAGTGCAC-3′
Hsp105ΔL (a.a. 1–511 + a.a. 605–858)
Sense: 5′-GGGAGAGACCTTCTTAACATGTATATTG-3′
Antisense: 5′-AGAGGAGCCATCCTCTTCCTCGGT-3′
Expression in bacterial cell
Hsp105Δβ
Sense: 5′-CTCGAGGCAGACATGGAATGTCCA-3′
Antisense: 5′-AGAAAGAATTGCACACTGCAGTGCAC-3′
Hsp105ΔβL
Sense: 5′-GGGAGAGACCTTCTTAACATGTATATTG-3′
Antisense: 5′-AGAAAGAATTGCACACTGCAGTGCAC-3′
Hsp105ΔL
Sense: 5′-GGGAGAGACCTTCTTAACATGTATATTG-3′
Antisense: 5′-AGAGGAGCCATCCTCTTCCTCGGT-3′

vitro assays (25), in cultured mammalian cells (26–31), in a *Drosophila* model (32) and in transgenic mice (33, 34). Hsp27 was also identified as a suppressor of polyglutamine-mediated cell death using a cellular model of Huntington's disease (35). However, because Hsp70/40 and Hsp27 suppressed polyglutamine-mediated death without suppressing polyglutamine aggregation in some experimental systems (35, 36), elucidation of the ways in which Hsps protect cells against polyglutamine mutations might be of relevance for other neurodegenerative conditions in which pathology is associated with protein deposition in neuronal cells.

Hsp105α is highly conserved in organisms from yeast to human (37–42) and is expressed in various tissues of mammals, but especially at high levels in brain (43). Recently, Hsp105α was demonstrated to have antiapoptotic properties for neuronal survival (44). Furthermore, Hsp105α prevents the aggregation of thermal denatured protein *in vitro* (45). However, its role in polyglutamine-mediated cell death/toxicity has not been studied. In the present study, we examined the role of Hsp105α in the context of polyglutamine aggregation and cell death using a cellular model of SBMA and demonstrate that Hsp105α without chaperone activity protects cells against polyglutamine-mediated cell death by reducing polyglutamine-protein aggregation. These findings suggest an important role for Hsp105α in preventing neurodegenerative diseases associated with polyglutamine expansions.

EXPERIMENTAL PROCEDURES

Plasmids—We used constructs expressing the N-terminal fragment of the AR fused to green fluorescence protein (GFP) containing 24, 65, or 97 CAG repeats (tAR24, tAR65, and tAR97, respectively) as a cellular model of SBMA (29), human Hsp70 (pCMV-Hsp70) (46), and Hsp40

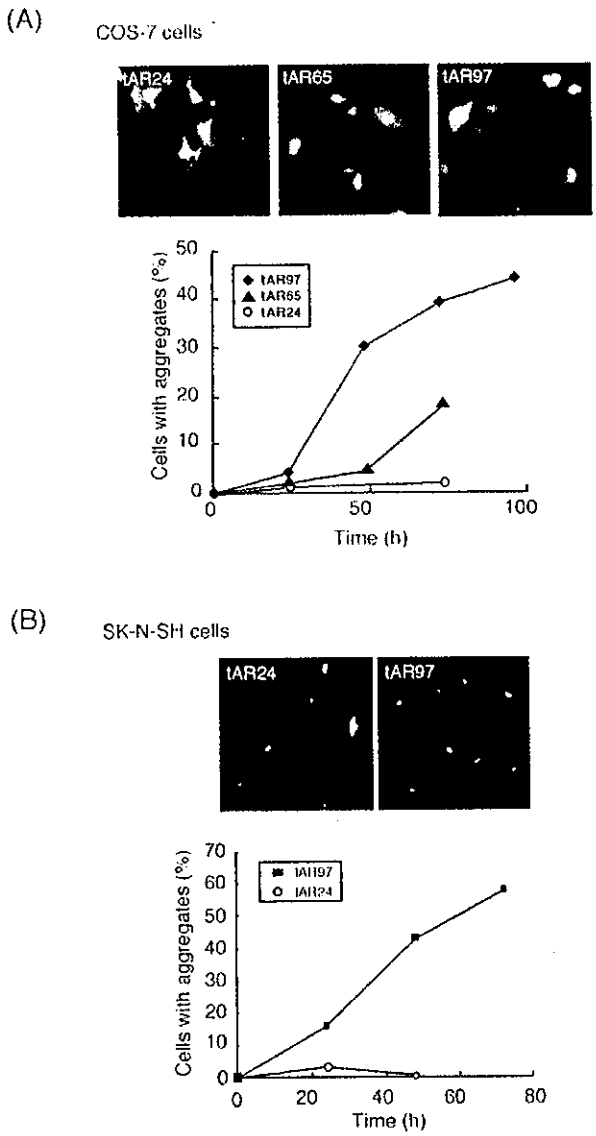

FIG. 1. **Truncated AR containing an expanded polyglutamine tract is accumulated as aggregates in COS-7 and SK-N-SH cells.** Expression plasmids for N-terminal fragments of AR containing various lengths of polyglutamine tract (tAR24, tAR65, and tAR97, 0.5 μg each) were transiently introduced into COS-7 (*A*) or SK-N-SH cells (*B*), and the cells were incubated further for 72 h. Each *upper panel* shows typical images of fluorescence of GFP which is fused to the C terminus of truncated AR, and each *lower graph* represents the rates of cells with aggregates *versus* GFP-positive cells at various times after transfection. Values represent the mean of duplicate experiments.

(pRC-Hsp40) (29) in mammalian cells. The constructs expressing Hsp105α (pcDNA105α) and Myc-epitope/His-tagged Hsp105α (pcDNA105α-mycHis) in mammalian cells were generated by ligating a full-length mouse Hsp105α cDNA (38) into pcDNA3.1 (Invitrogen) at *Bam*HI and *Eco*RI sites and pcDNA3.1(+)-mycHis vector (Invitrogen) at *Xba*I and *Kpn*I sites, respectively. The constructs expressing Hsp105N1–N3, Δβ, ΔL, and ΔβL in mammalian cells were generated by self-ligation of DNA made by PCR using pcDNA105α-mycHis (Hsp105N1–N3) or pcDNA105α (Hsp105Δβ, ΔL, ΔβL, and C1–C3) as template DNA and a specific set of primers (Table I).

We used a construct expressing GST- and HA-tagged tAR65 (GST-tAR65-HA) in bacterial cells (47). The constructs expressing HSP105α deletion mutants in bacterial cells were generated by ligating insert DNA made by PCR using pTrcHis105-1 (45) as a template DNA and a specific set of primers (Table I) into pTrcHisA vector (Invitrogen) at the *Kpn*I site.

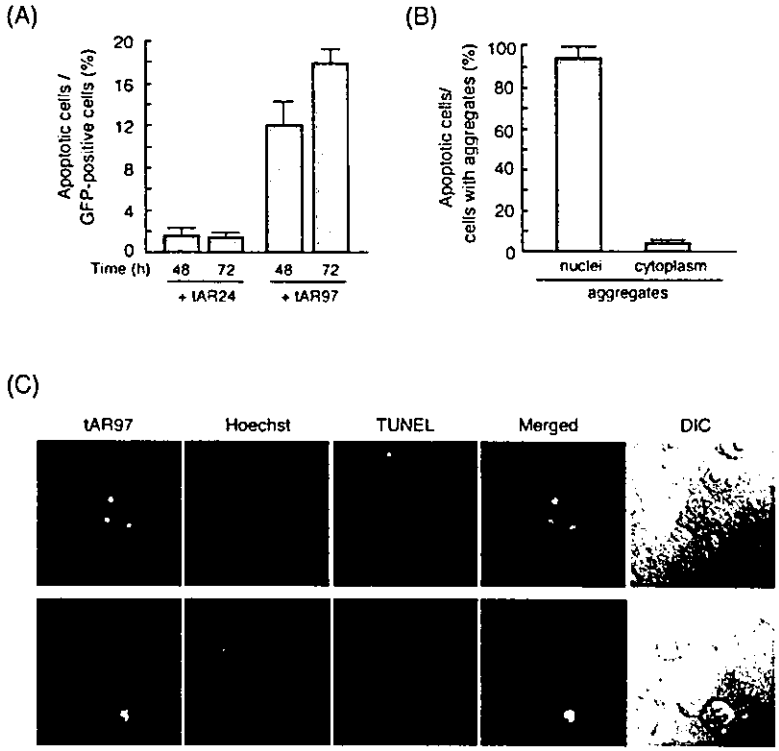

FIG. 2. **Apoptosis occurs in cells with intranuclear aggregates.** *A*, COS-7 cells were transfected with the expression plasmid for tAR24 (+ *tAR24*) or tAR97 (+ *tAR97*) and incubated further for 48 or 72 h. Then cells were fixed and stained with Hoechst 33342. Rates of cells with condensed chromatin *versus* GFP-positive cells are presented. *B*, COS-7 cells were transfected with the expression plasmid for tAR97 and incubated further for 72 h. Rates of apoptotic cells *versus* cells with aggregates in nuclei and/or cytoplasms are presented. Values in *A* and *B* represent the mean ± S.D. of three independent experiments. *C*, fragmentation of DNA in nuclei was evaluated by TUNEL methods 72 h after the transfection of tAR97. *DIC* represents a difference interference contrast image of cells.

Cell Culture and Transfection—African green monkey kidney cells (COS-7) and human neuroblastoma cells (SK-N-SH) were supplied from Riken cell bank. COS-7 cells were maintained in Dulbecco's modified Eagle's medium (Nissui Pharmaceutical) supplemented with 10% fetal bovine serum. SK-N-SH cells were maintained in α-minimal essential medium (Invitrogen) with 10% fetal bovine serum. For transfection of plasmid DNA, cells were grown on coverslips to 70–80% confluence and washed twice with Opti-MEM (Invitrogen). Then plasmid DNA was transfected into cells with DMRIE-C reagent (Invitrogen) for 14–18 h, according to the manufacturer's instructions.

Indirect Immunofluorescence—COS-7 cells grown on coverslips were washed with phosphate-buffered saline without Ca^{2+} and Mg^{2+} (PBS(−)) and fixed with 4% paraformaldehyde for 30 min at room temperature. These cells were washed with PBS(−) and incubated with blocking solution containing 3% bovine serum albumin (BSA) in PBS(−) at room temperature for 1 h. Then rabbit anti-human Hsp105 (48) or mouse anti-Hsp70 monoclonal antibody (Sigma) at a 1:300 dilution was added to the coverslips and incubated in a moist chamber at 37 °C for 1 h. After a wash with PBS(−), rhodamine-conjugated goat anti-rabbit or mouse IgG antibody (Molecular Probes) at a 1:50 dilution was added to the coverslips, and they were incubated further at 37 °C for 1 h. After another wash with PBS(−), cells were observed using a confocal laser scanning microscope (Zeiss).

Analysis of Aggregation in Vivo—COS-7 cells transfected with expression plasmid for tAR24, tAR65, or tAR97 were washed with PBS(−) and fixed with 4% paraformaldehyde for 30 min at room temperature. Cells on coverslips were washed with PBS(−) and stained with 10 μM Hoechst 33342 for 15 min at room temperature. The cells were washed with PBS(−) and then examined using a confocal laser scanning microscope. The number of transfected cells with visible aggregates and the number of transfected cells without aggregates were counted independently in randomly chosen microscopic fields in different areas of a coverslip. Approximately 300–600 transfected cells were analyzed for data in each experiment.

Detection of the Apoptotic Cells—The apoptotic cells were identified by their nuclear morphology and the terminal nucleotidyl transferase-mediated UTP nick end labeling (TUNEL) method (29). Nuclear morphology was examined by staining with Hoechst 33342. The TUNEL method was performed using a DeadEnd™ apoptosis detection kit (Promega) according to the manufacturer's instructions. Briefly, cells were fixed with 4% paraformaldehyde at 72 h after transfection. Fixed cells were incubated with biotinylated deoxynucleotides, then stained with streptavidin-rhodamine conjugate (Molecular Probes) and Hoechst 33342. Cells were then observed by confocal laser scan microscopy.

Western Blotting Analysis—Cells were lysed with a solution containing 0.1% SDS at 72 h after transfection. The cellular proteins (15 μg) were separated by 7.5% SDS-PAGE and blotted onto a nitrocellulose membrane. The membrane was incubated with rabbit anti-human Hsp105 (37) or mouse anti-Hsp70 (Sigma) antibody, then incubated with horseradish peroxidase-conjugated anti-rabbit IgG (Santa Cruz) for Hsp105 or anti-mouse IgG (Santa Cruz) for Hsp70 at a 1:2,000 dilution. These proteins were detected using the enhanced chemiluminescence (ECL) detection system (Amersham Biosciences).

Protein Purification—GST-tAR65-HA was expressed in BL21 bacterial cells on addition of 1 mM isopropyl-β-D-thiogalactopyranoside. Cells were collected and resuspended in ice-cold TEGM buffer (10 mM Tris-HCl, pH 7.4, 1 mM EDTA, 10% glycerol, and 10 mM sodium molybdate). Cells were then sonicated for 1 min and centrifuged for 30 min at 10,000 × *g*. To purify GST-tagged proteins, the supernatants were mixed with glutathione-Sepharose 4B (Amersham Biosciences) and incubated at 4 °C for 1 h. The Sepharose beads were then washed with PBS(−) and eluted with 10 mM reduced glutathione. Wild-type Hsp105α and its mutants were purified as His-tagged proteins by successive Ni^{2+}-agarose (Invitrogen) and Mono Q anion exchange column (Amersham Biosciences) chromatographies, as described previously (45).

Detection of Aggregates of Truncated AR in Vitro—GST-tAR65-HA (1 μM) was incubated with Hsp105α, its mutants, or BSA in 20 μl of buffer A (25 mM Tris-HCl, pH 7.5, 150 mM NaCl, 1 mM dithiothreitol, and 1 mM phenylmethylsulfonyl fluoride) at 30 °C for 12 h in the presence of 2 mM ADP. The reaction was stopped by the addition of 20 μl of a solution containing 2% SDS and 100 mM dithiothreitol, and the mixtures were heated at 98 °C for 5 min. After the addition of 200 μl of a 1% SDS solution, the mixture was filtered through a 0.2-μm cellulose acetate membrane (Advantec). Aggregates on the membrane were incubated with anti-HA tag antibody (1:500, Santa Cruz) then with peroxidase-conjugated anti-mouse IgG antibody (1:2000) and detected with an ECL detection system (Santa Cruz).

Immunohistochemistry—We perfused 20 ml of a 4% paraformaldehyde fixative in 0.1 M phosphate buffer, pH 7.4, through the left cardiac ventricle of SBMA transgenic mice (49) deeply anesthetized with ketamine-xylazine, postfixed tissues overnight in 10% phosphate-buffered formalin, and processed tissues for paraffin embedding. Then, 4-μm thick tissue sections were deparaffinized, dehydrated with alcohol, and

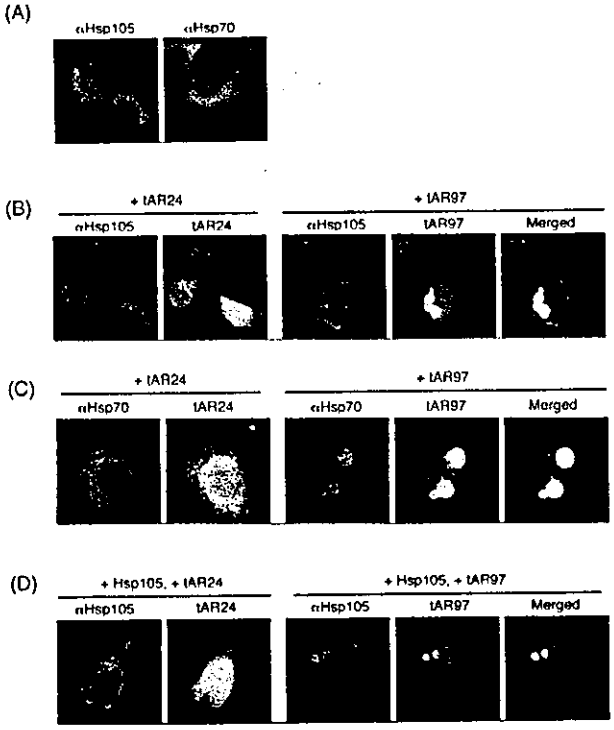

FIG. 3. **Localization of Hsp105α and Hsc70/Hsp70 in COS-7 cells with tAR97 aggregates.** *A*, control COS-7 cells were fixed, and endogenous Hsp105α (*red*) or Hsp70 (*red*) was detected by indirect immunofluorescence using anti-Hsp105 or anti-Hsp70 antibody, respectively. Nuclear morphology (*blue*) was detected by staining with Hoechst 33342. *B* and *C*, COS-7 cells were transfected with the expression plasmid for tAR24 (+ *tAR24*) or tAR97 (+ *tAR97*) and incubated further for 72 h. tAR24 or tAR97 (*green*) was detected by the green fluorescence of GFP, and endogenous Hsp105α (*red*) (*B*) and Hsp70 (*red*) (*C*) were detected by indirect immunofluorescence. Nuclear morphology (*blue*) was observed by staining with Hoechst 33342. *D*, COS-7 cells were cotransfected with expression plasmids for Hsp105α and tAR24 (+ *Hsp105*, + *tAR24*) or Hsp105α and tAR97 (+ *Hsp105*, + *tAR97*) and incubated further for 72 h. Nuclear morphology (*blue*) stained with Hoechst 33342 and tAR97 (*green*) and Hsp105α (*red*) by indirect immunofluorescence was observed.

treated in formic acid for 5 min at room temperature and with trypsin (Dako) for 20 min at 37 °C. The tissue sections were blocked with normal goat serum (1:20) and incubated with rabbit anti-mouse Hsp105 antibody (1:100). The sections were incubated with biotinylated goat anti-rabbit IgG (Vector Laboratories), and immune complexes were visualized using streptavidin-horseradish peroxidase (Dako) and 3,3'-diaminobenzidine (Dojindo) substrate and counterstained with methyl green. For the immunohistochemistry of tissues of SBMA patients, paraffin-embedded sections of the spinal cord and scrotal skin from nine patients with clinicopathologically and genetically confirmed SBMA (age 51–84 years, mean 64.3 years) were examined using rabbit anti-human Hsp105 antibody (1:100).

RESULTS

Aggregation of Truncated AR with an Expanded Polyglutamine Tract and Induction Apoptosis in COS-7 and SK-N-SH Cells—Truncated ARs containing 24, 65, or 97 polyglutamine repeats (tAR24, tAR65, or tAR97, respectively) were transiently expressed in non-neuronal (COS-7) and neuronal cells (SK-N-SH) (Fig. 1). Because these tAR constructs were connected with GFP at the C terminus, the cellular localization of these chimerical peptides was detected by fluorescence microscopy. tAR65 or tAR97, but not tAR24, aggregated in cytoplasm and/or nucleus in non-neuronal COS-7 cells as well as neuronal SK-N-SH cells, as shown previously in the neuronal Neuro2a cell line (29). Proportions of cells with aggregates increased depending on the incubation time after transfection and polyglutamine repeat length. Approximately 45 and 60% of GFP-positive cells had aggregates in the COS-7 and SK-N-SH cell lines, respectively, at 72 h after transfection of the expression plasmid for tAR97. Among the cells with aggregates of tAR97, intranuclear aggregates were detected in 40 and 8% of transfected COS-7 and SK-N-SH cells, respectively (data not shown).

Under these conditions, apoptotic cells with condensed chromatin were observed in 12 and 18% of all COS-7 cells expressing GFP at 48 and 72 h after transfection of the expression plasmid for tAR97, respectively (Fig. 2*A*). In contrast, cells expressing tAR24 showed little apoptotic morphology after the transfection (Fig. 2*A*). Most apoptotic cells had aggregates of tAR97 in the nucleus, whereas cells containing cytoplasmic aggregates exhibited few apoptotic features (Fig. 2*B*). Furthermore, when the presence of fragmented DNA was assessed by the TUNEL method, the cells with intranuclear aggregates, but not cells with cytoplasmic aggregates, were found to be positive (Fig. 2*C*). These findings suggested that the intranuclear aggregates induced apoptosis in COS-7 cells. Similar results were obtained with SK-N-SH cells (data not shown). Thus, although both non-neuronal and neuronal cells could be utilized as a cell model of SBMA, we used the COS-7 model for further study because the cells expressed the transfected plasmids markedly well.

Colocalization of Hsp105α and Hsp70 with Aggregates of Truncated AR—We next examined the cellular distribution of Hsp105α and Hsp70 in COS-7 cells by indirect immunofluorescence using anti-human Hsp105 and anti-Hsp70 antibodies. Under nonstressed conditions, endogenous Hsp105α and Hsc70/Hsp70 were localized mainly in the cytoplasm of cells (Fig. 3*A*). When tAR24 was transiently expressed in COS-7 cells, both endogenous Hsp105α and Hsp70 were also detected in the cytoplasm of the cells (Fig. 3, *B* and *C*). In contrast, when tAR97 was transiently expressed in COS-7 cells, endogenous Hsp70 was colocalized to the aggregates of tAR97, whereas endogenous Hsp105α was not. However, when overexpressed with tAR97 in cells, Hsp105α was colocalized to the aggregates of tAR97 (Fig. 3*D*), whereas Hsp105α was localized to the cytoplasm of cells in which tAR97 was not expressed. Thus, the increased amounts of Hsp105α in cells seemed necessary for the interaction with and binding to the tAR containing an expanded polyglutamine tract.

Overexpression of Hsp105α Reduced Aggregation of tAR97—Hsp105α prevents the aggregation of denatured protein *in vitro* (45) and suppresses apoptotic cell death induced by various forms of stress in neuronal PC12 cells (44). Because the overexpressed Hsp105α colocalized to intracellular aggregates of tAR97 (Fig. 3), we next examined the effects of Hsp105α on the aggregation of tAR containing an expanded polyglutamine tract. When expression plasmids for Hsp105α and tAR97 were cotransfected into COS-7 cells, the proportion of cells with tAR97 aggregates was reduced to ~50% of that transfected without Hsp105α (Fig. 4, *A* and *B*). Overexpression of Hsp70 or Hsp40 also suppressed the formation of aggregates similarly to Hsp105α, and Hsp70 and Hsp40 in combination suppressed the formation strongly. However, the suppression of aggregation by Hsp70 and Hsp40 was not enhanced by the coexpression of Hsp105α.

When cellular toxicity was analyzed by examining the nuclear morphology of cells stained with Hoechst 33342, numbers of apoptotic cells with condensed chromatin were found to be markedly reduced by coexpression of Hsp105α with tAR97 (Fig. 4*C*). Overexpression of Hsp70 and/or Hsp40 also suppressed apoptotic cell death caused by expression of tAR97. Furthermore, when various amounts of Hsp105α were coexpressed

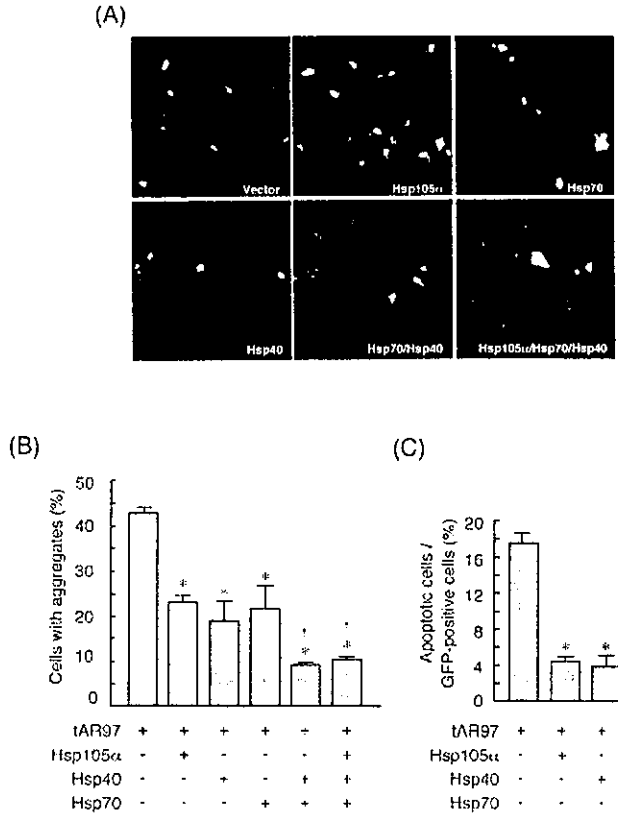

FIG. 4. **Effects of Hsp105α on aggregation of tAR97.** *A*, COS-7 cells were cotransfected with expression plasmids for tAR97 (0.5 μg) and pcDNA3.1 vector, Hsp105, Hsp70, and/or Hsp40 (1 μg each) and incubated further for 72 h. Typical images of fluorescence of GFP are shown. *B*, rates of cells with aggregates *versus* GFP-positive cells are shown. *C*, rates of apoptotic cells with condensed chromatin *versus* GFP-positive cells are shown. Values in *B* and *C* represent the mean ± S.D. of three independent experiments. Statistical significance was determined using Student's *t* test; *, $p < 0.01$ *versus* control with vector. †, $p < 0.01$ *versus* cells overexpressing Hsp70 or Hsp40 alone.

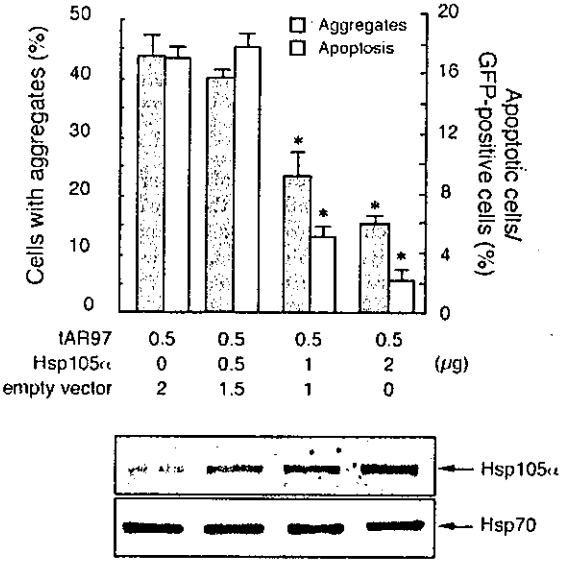

FIG. 5. **Hsp105α suppresses aggregation of tAR97 and cellular toxicity in a dose-dependent manner.** The expression plasmids for empty vector, Hsp105α, and/or tAR97 were introduced into COS-7 cells, and the cells were incubated further for 72 h. GFP fluorescence was observed using a confocal laser scan microscope. Rates of cells with aggregates or apoptotic cells/GFP-positive cells are shown as *closed* or *opened bars*, respectively. Values represent the mean ± S.D. of three independent experiments. Statistical significance was determined using Student's *t* test; *, $p < 0.01$ *versus* control with vector. *Lower panels* show Western blots of Hsp105α and Hsp70 in the cells.

with tAR97, the aggregation of tAR97 and apoptosis were both suppressed depending on cellular levels of Hsp105α (Fig. 5). Under these conditions, cellular levels of endogenous Hsp70 were not changed by overexpression of Hsp105α (Fig. 5, *lower panel*). These findings strongly suggested that when overexpressed, Hsp105α suppressed effectively not only the formation of aggregates but also the expanded polyglutamine-mediated cellular toxicity.

Identification the Domain of Hsp105α Required for Suppression of tAR97 Aggregation—Hsp105α is composed of N-terminal ATP binding, central β-sheet, loop and C-terminal α-helix domains, similar to the Hsp70 family proteins. To determine the domain of Hsp105α essential to suppress the aggregation caused by expansion of the polyglutamine tract, we constructed expression plasmids for various deletion mutants of Hsp105α, as shown in Fig. 6*A*. When coexpressed with tAR97 in COS-7 cells, the Hsp105α mutant C3 or ΔL significantly suppressed the aggregation of tAR97 as did wild-type Hsp105α (Fig. 6*B*). However, other deletion mutants failed to suppress the aggregation of tAR97. Because the C3 and ΔL mutants contain both β-sheet and α-helix domains, these domains seemed to be essential to suppress the aggregation caused by expansion of the polyglutamine tract.

Hsp105α Inhibits Aggregation of GST-tAR65 in Vitro—To examine further whether Hsp105α can directly suppress aggregation of the expanded polyglutamine tract, we analyzed the effects of Hsp105α on the aggregation of tAR65 *in vitro* (Fig. 7). GST-tAR65-HA was incubated with or without Hsp105α or its mutant, and insoluble aggregates that formed during the incubation were collected on cellulose acetate membranes. Hsp105α suppressed the aggregation of tAR65 in a dose-dependent manner (Fig. 7*A*). Furthermore, the aggregation was suppressed by wild-type Hsp105α and the mutants C3 and ΔL but not by other deletion mutants (Fig. 7*B*). Thus, it was suggested that Hsp105α itself suppressed the aggregation of truncated AR containing an expanded polyglutamine without other cellular components and that both the β-sheet and

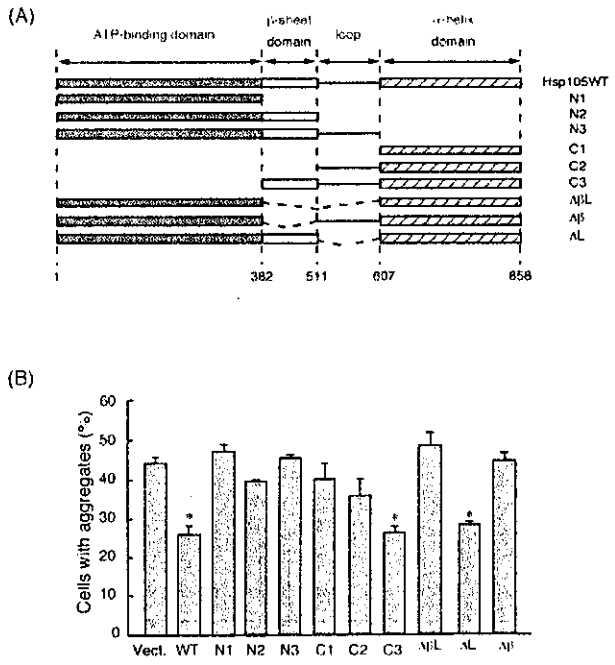

FIG. 6. **Domain of Hsp105α required for suppression of aggregation of tAR97.** *A*, schematic diagram of deletion mutants of Hsp105α. *B*, COS-7 cells were cotransfected with expression plasmid for tAR97 and deletion mutant of Hsp105α and incubated further for 72 h. GFP fluorescence was observed using a confocal laser scan microscope. Rates of cells with aggregates *versus* GFP-positive cells are shown. Values represent the mean ± S.D. of three independent experiments. Statistical significance was determined using Student's *t* test; *, $p < 0.01$ *versus* control with vector.

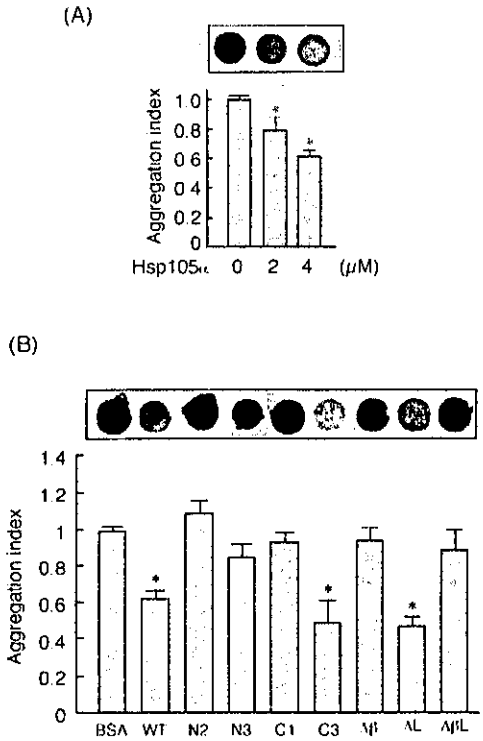

FIG. 7. **Hsp105α inhibits the aggregation of tAR65 *in vitro*.** *A*, 1 μM GST-tAR65-HA was incubated with 2 or 4 μM Hsp105α or 4 μM BSA at 25 °C for 16 h. *B*, 1 μM GST-tAR65-HA was incubated with Hsp105α, various deletion mutants of Hsp105α, or BSA (4 μM each) at 25 °C for 16 h. Then, aggregates were trapped on cellulose acetate membranes and detected by immunoblotting using anti-HA antibody. Densities of spots were quantified, and relative rates of tAR65 retained on membranes are shown as an aggregation index. Values represent the mean ± S.D. of three independent experiments. Statistical significance was determined using Student's *t* test; *, $p < 0.01$ *versus* control with BSA.

α-helix domains of Hsp105α seemed necessary for the suppression *in vitro* as well as *in vivo*.

Immunohistochemistry of Hsp105α in Nuclear Inclusions in the Tissues of SBMA Patients and Transgenic Mice—Nuclear inclusions containing mutant and truncated AR with an expanded polyglutamine have been shown to occur in residual motor neurons in the brain stem and spinal cord (4) and also in the skin, testis, and some other visceral organs of SBMA patients (5). We next examined whether Hsp105α localizes in the nuclear inclusions in these tissues of SBMA patients. As shown in Fig. 8, *A* and *B*, Hsp105α staining was observed in nuclear inclusions in neurons of the spinal anterior horn and scrotal skin epidermal cells. Furthermore, when male transgenic mice carrying a full-length AR with an expanded polyglutamine (97 repeats) tract and showing neuropathologic changes equivalent to human SBMA (49) were examined immunohistochemically, Hsp105α was also detected in nuclear inclusions in neurons of the spinal anterior horn and muscle cells (Fig. 8, *C* and *D*). However, although Hsp105α was commonly observed in nuclear inclusions in scrotal skin epidermal cells of SBMA patients and in muscle cells of the transgenic mice, only a few Hsp105-immunoreactive nuclear inclusions were observed in neurons of the spinal anterior horn of either patients or mice.

DISCUSSION

Hsp105α is a stress protein expressed at an especially high level in mammalian brain (43) and has an antiapoptotic effect in neuronal cells (44). Hsp105α prevents the aggregation of denatured proteins caused by heat shock *in vitro* but has not been shown to have chaperone activity (45). Here, we showed that Hsp105α suppressed not only the formation of intracellular aggregates but also apoptosis caused by an expansion of the polyglutamine tract in a cellular model of SBMA. Hsp105α is composed of N-terminal ATP binding, central β-sheet, loop, and C-terminal α-helix domains, similar to the Hsp70 family proteins. For the suppression of aggregation of truncated AR containing an expanded polyglutamine tract, β-sheet and α-helix domains of Hsp105α were essential *in vivo* and *in vitro*. Hsp70 binds unfolded proteins at the β-sheet domain and prevents aggregation of denatured proteins (50), and the α-helix domain is essential for stable binding to the substrate protein (50). Recently, we found that the β-sheet domain of Hsp105α could bind to denatured proteins.[2] Because Hsp105α mutants with β-sheet but not α-helix domains did not prevent the aggregation of truncated AR containing an expanded polyglutamine tract *in vivo* and *in vitro*, the α-helix domain may be necessary for stabilization of the Hsp105α-substrate complexes as is Hsp70.

Hsp70 and Hsp40 have recently been identified as important regulators of polyglutamine aggregation and/or cell death in cellular models of polyglutamine disease (29). Hsp70 promotes protein folding by an ATP-dependent process involving polypeptide segments enriched in hydrophobic residues (50, 51) and cooperates in this function with members of the Hsp40 family (52). The binding of Hsp70 to substrate proteins may prevent protein aggregation directly by shielding the interactive surfaces of nonnative polypeptides. Suppression of polyglutamine-induced neurotoxicity by expression of Hsp40 alone

[2] N. Yamagishi, K. Ishihara, and T. Hatayama, unpublished data.

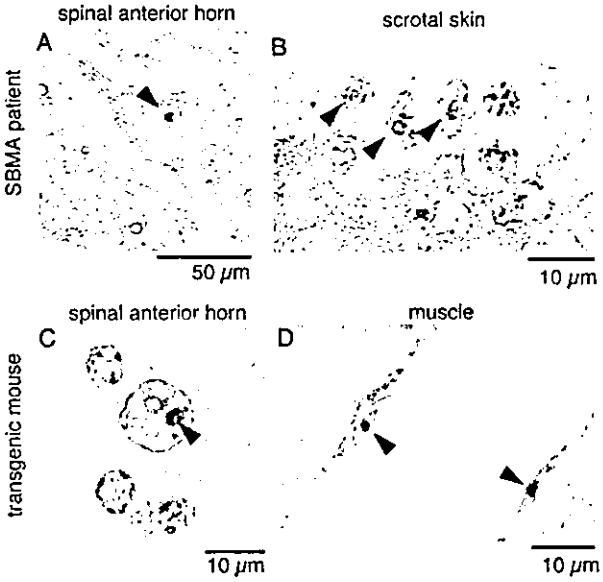

FIG. 8. **Immunohistochemistry of Hsp105α in nuclear inclusions in the tissues of patients and transgenic mice with SBMA.** Tissue sections of spinal anterior horn (*A*) and scrotal skin (*B*) from SBMA patients or spinal anterior horn (*C*) and muscle (*D*) from male AR-Q97 transgenic mice were examined using anti-human Hsp105 or rabbit anti-mouse Hsp105 antibody, respectively, and counterstained with methyl green. *Arrowheads* indicate nuclear inclusions.

is most likely caused by the ability to activate the endogenous Hsp70 for suppression of the neurotoxicity. Here, we showed that overexpression of Hsp105α alone suppressed the aggregation of truncated AR containing an expanded polyglutamine tract similarly to Hsp70 or Hsp40, whereas Hsp70 and Hsp40 in combination suppressed the aggregation much more markedly. However, because the suppression of aggregation by Hsp70 and Hsp40 was not enhanced by the coexpression of Hsp105α, Hsp105α and Hsp70/Hsp40 seem to suppress the polyglutamine-induced neurotoxicity by similar mechanisms.

In polyglutamine diseases such as spinocerebellar ataxia type 3/Machado-Joseph disease, Hsp70 colocalizes in intracellular aggregates, whereas Hsp105α is not found in the aggregates (27). In the present study, Hsp105 was detected in nuclear inclusions in neurons of the spinal anterior horn and scrotal skin epidermal cells of SBMA patients and also in neurons of the spinal anterior horn and muscle cells of SBMA transgenic mice, although only a few Hsp105-immunoreactive nuclear inclusions were observed in neurons of the spinal cord of the patients and mice. On the other hand, in a cellular model of SBMA, endogenous Hsp70 but not endogenous Hsp105α localized to aggregates of tAR97, although the overexpressed Hsp105α localized to the aggregates of tAR97. Because Hsp70 exists in much larger amounts than Hsp105α in cells, Hsp70 may interact preferentially with truncated AR containing an expanded polyglutamine tract. However, when Hsp105α was overexpressed in the cells, reaching high levels, it seemed to bind and localize to truncated AR containing an expanded polyglutamine tract like Hsp70. Thus, the existence of molecular chaperones at high concentrations in cells may be essential to prevent the aggregation of truncated AR containing an expanded polyglutamine tract.

The intranuclear aggregation of truncated AR containing an expanded polyglutamine tract and apoptotic cell death coincided in the cellular model of SBMA, and both processes were suppressed by overexpression of Hsp105α. As to the mechanism by which Hsp105α suppresses the apoptosis caused by expansion of the polyglutamine tract, one possibility is that suppression of aggregation by Hsp105α mediates suppression of apoptosis. Key components of the transcription apparatus, such as cAMP response element binding protein-binding protein, p53, and $TAF_{II}130$, are sequestered in polyglutamine-containing inclusions, then the expanded polyglutamine tract causes altered gene transcription (30, 53–57). By preventing the formation of intranuclear aggregates, Hsp105α may suppress the alteration of gene transcription caused by an expanded polyglutamine tract and eventually apoptotic cell death.

Another possibility is that the abilities of Hsp105α to suppress aggregate formation and cellular toxicity caused by expansion of the polyglutamine tract are independent. Recently, molecular chaperones, such as Hsp70, Hsp40, and Hsp27, were shown to suppress an expanded polyglutamine-mediated cellular toxicity independently of suppression of aggregation (35, 36). Although the relationship between the aggregation and the induction of apoptosis remains unknown, the suppression of cellular toxicity by molecular chaperones may be caused by the ability to inhibit apoptosis. Hsp105α suppresses heat shock-induced apoptosis in neuronal cells by preventing the activation of c-Jun N-terminal kinase (44). Because c-Jun N-terminal kinase is activated by the expanded polyglutamine tract (58), Hsp105α may also suppress the cellular toxicity by its ability to inhibit apoptosis.

In conclusion, we identified Hsp105α as a novel molecule that reduces aggregation and cellular toxicity caused by an expansion of the polyglutamine tract. Molecular chaperones, such as Hsp105α, Hsp70, Hsp40, and Hsp27, seem to suppress cell toxicity caused by an expansion of the polyglutamine tract. These findings suggest that increasing the expression levels or enhancing the function of chaperones in neurons may open up a promising approach to the treatment of polyglutamine diseases, although more studies are required to determine the precise mechanism of neurodegeneration of CAG repeat diseases.

REFERENCES

1. Kennedy, W. R., Alter, M., and Sung, J. H. (1968) *Neurology* 18, 671–680
2. Sobue G., Hashizume, Y., Mukai, E., Hirayama, M., Mitsuma, T., and Takahashi, A. (1989) *Brain* 112, 209–232
3. La Spada, A. R., Wilson, E. M., Lubahn, D. B., Harding, A. E., and Fischbeck, K. H. (1991) *Nature* 352, 77–79
4. Li, M., Miwa, S., Kobayashi, Y., Merry, D. E., Yamamoto, M., Tanaka, F., Doyu, M., Hashizume, Y., Fischbeck, K. H., and Sobue, G. (1998) *Ann. Neurol.* 44, 249–254
5. Li, M., Nakagomi, Y., Kobayashi, Y., Merry, D. E., Tanaka, F., Doyu, M., Mitsuma, T., Hashizume, Y., Fischbeck, K. H., and Sobue, G. (1998) *Am. J. Pathol.* 153, 695–701
6. The Huntington's Disease Collaborative Research Group (1993) *Cell* 72, 971–983
7. Koide, R., Ikeuchi, T., Onodera, O., Tanaka, H., Igarashi, S., Endo, K., Takahashi, H., Kondo, R., Ishikawa, A., Hayashi, T., Saito, M., Tomoda, A., Miike, T., Naito, H., Ikuta, F., and Tsuji, S. (1994) *Nat. Genet.* 6, 9–13
8. Nagafuchi, S., Yanagisawa, H., Sato, K., Shirayama, T., Ohsaki, E., Bundo, M., Takeda, T., Tadokoro, K., Kondo, I., Murayama, N., Tanaka, Y., Kikushima, H., Umino, K., Kurosawa, H., Furukawa, T., Nihei, K., Inoue, T., Sano, A., Komura, O., Takahashi, M., Yoshizawa, T., Kanazawa, I., and Yamada, M. (1994) *Nat. Genet.* 6, 14–18
9. Kawaguchi, Y., Okamoto, T., Taniwaki, M., Aizawa, M., Inoue, M., Katayama, S., Kawamaki, H., Nakamura, S., Nishimura, M., Akiguchi, I., Kimura, J., Narumiya, S., and Kakizuka, A. (1994) *Nat. Genet.* 8, 221–228
10. Orr, H. T., Chung, M. Y., Banfi, S., Kwiatkowski, T. J., Servadio, A., Beaudet, A. L., McCall, A. E., Duvick, L. A., Ranum, L. P., and Zoghbi, H. Y. (1993) *Nat. Genet.* 4, 221–226
11. Pulst, S. M., Nechiporuk, A., Nechiporuk, T., Gispert, S., Chen, X. N., Lopes-Cendes, I., Pearlman, S., Starkman, S., Orozco-Diaz, G., Lunkes, A., DeJong, P., Rouleau, G. A., Auburger, G., Korenberg, J. R., Figueroa, C., and Sahba, S. (1996) *Nat. Genet.* 14, 269–276
12. Sanpei, K., Takano, H., Igarashi, S., Sato, T., Oyake, M., Sasaki, H., Wakisaka, A., Tashiro, K., Ishida, Y., Ikeuchi, T., Koide, R., Saito, M., Sato, A., Tanaka, T., Hanyu, S., Takiyama, Y., Nishizawa, M., Shimizu, N., Nomura, Y., Segawa, M., Iwabuchi, K., Eguchi, I., Tanaka, H., Takahashi, H., and Tsuji, S. (1996) *Nat. Genet.* 14, 277–284
13. Imbert, G., Saudou, F., Yvert, G., Devys, D., Trottier, Y., Garnier, J. M., Weber, C., Mandel, J. L., Cancel, G., Abbas, N., Durr, A., Didierjean, O., Stevanin, G., Agid, Y., and Brice, A. (1996) *Nat. Genet.* 14, 285–291

14. Zhuchenko, O., Bailey, J., Bonnen, P., Ashizawa, T., Stockton, D. W., Amos, C., Dobyns, W. B., Subramony, S. H., Zoghbi, H. Y., and Lee, C. C. (1997) *Nat. Genet.* **15**, 62–69
15. David, G., Abbas, N., Stevanin, G., Durr, A., Yvert, G., Cancel, G., Weber, C., Imbert, G., Saudou, F., Antoniou, E., Drabkin, H., Gemmill, R., Giunti, P., Benomar, A., Wood, N., Ruberg, M., Agid, Y., Mandel, J. L., and Brice, A. (1997) *Nat. Genet.* **17**, 65–70
16. Welch, W. J., and Gambetti, P. (1998) *Nature* **392**, 23–24
17. Sherman, M. Y., and Goldberg, A. L. (2001) *Neuron* **29**, 15–32
18. Johnston, J. A., Ward, C. L., and Kopito, R. R. (1998) *J. Cell Biol.* **143**, 1883–1898
19. Schulz, J. B., and Dichgans, J. (1999) *Curr. Opin. Neurol.* **12**, 433–439
20. Heiser, V., Scherzinger, E., Boeddrich, A., Nordhoff, E., Lurz, R., Schugardt, N., Lehrach, H., and Wanker, E. E. (2000) *Proc. Natl. Acad. Sci. U. S. A.* **97**, 6739–6744
21. Kazemi-Esfarjani, P., and Benzer, S. (2000) *Science* **287**, 1837–1840
22. Nagai, Y., Tucker, T., Ren, H., Kenan, D. J., Henderson, B. S., Keene, J. D., Strittmatter, W. J., and Burke, J. R. (2000) *J. Biol. Chem.* **275**, 10437–10442
23. Hendricks, J. P., and Hartl, F. U. (1993) *Annu. Rev. Biochem.* **62**, 349–384
24. Hartl, F. U. (1996) *Nature* **381**, 571–580
25. Muchowski, P. J., Schaffar, G., Sittler, A., Wanker, E. E., Hayer-Hartl, M. K., and Hartl, F. U. (2000) *Proc. Natl. Acad. Sci. U. S. A.* **97**, 7841–7846
26. Cummings, C. J., Mancini, M. A., Antalffy, B., DeFranco, D. B., Orr, H. T., and Zoghbi, H. Y. (1998) *Nat. Genet.* **19**, 148–154
27. Chai, Y., Koppenhafer, S. L., Bonini, N. M., and Paulson, H. L. (1999) *J. Neurosci.* **19**, 10338–10347
28. Jana, N. R., Tanaka, M., Wang, G., and Nukina, N. (2000) *Hum. Mol. Genet.* **9**, 2009–2018
29. Kobayashi, Y., Kume, A., Li, M., Doyu, M., Hata, M., Ohtsuka, K., and Sobue, G. (2000) *J. Biol. Chem.* **275**, 8772–8778
30. Stenoien, D. L., Cummings, C. J., Adams, H. P., Mancini, M. G., Patel, K., DeMartino, G. N., Marcelli, M., Weigel, N. L., and Mancini, M. A. (1999) *Hum. Mol. Genet.* **8**, 731–741
31. Wyttenbach, A., Carmichael, J., Swartz, J., Furlong, R. A., Narain, Y., Rankin, J., and Rubinsztein, D. C. (2000) *Proc. Natl. Acad. Sci. U. S. A.* **97**, 2898–2903
32. Warrick, J. M., Chan, H. Y., Gray-Board, G. L., Chai, Y., Paulson, H. L., and Bonini, N. M. (1999) *Nat. Genet.* **23**, 425–428
33. Cummings, C. J., Sun, Y., Opal, P., Antalffy, B., Mestril, R., Orr, H. T., Dillmann, W. H., and Zoghbi, H. Y. (2001) *Hum. Mol. Genet.* **10**, 1511–1518
34. Adachi, H., Katsuno, M., Minamiyama, M., Sang, C., Pagoulatos, G., Angelidis, C., Kusakabe, M., Yoshiki, A., Kobayashi, Y., Doyu, M., and Sobue, G. (2003) *J. Neurosci.* **23**, 2203–2211
35. Wyttenbach, A., Sauvageot, O., Carmichael, J., Diaz-Latoud, C., Arrigo, A. P., and Rubinsztein, D. C. (2002) *Hum. Mol. Genet.* **11**, 1137–1151
36. Zhou, H., Li, S. H., and Li, X. J. (2001) *J. Biol. Chem.* **276**, 48417–48424
37. Ishihara, K., Yasuda, K., and Hatayama, T. (1999) *Biochim. Biophys. Acta* **1444**, 138–142
38. Yasuda, K., Nakai, A., Hatayama, T., and Nagata, K. (1995) *J. Biol. Chem.* **270**, 29718–29723
39. Lee-Yoon, D., Easton, D., Murawski, M., Burd, R., and Subjeck, J. R. (1995) *J. Biol. Chem.* **270**, 15725–15733
40. Plesofsky-Vig, N., and Brambl, R. (1998) *J. Biol. Chem.* **273**, 11335–11341
41. Storozhenko, S., De Pauw, P., Kushnir, S., Van Montagu, M., and Inze, D. (1996) *FEBS Lett.* **390**, 113–118
42. Mukai, H., Kuno, T., Tanaka, H., Hirata, D., Miyakawa, T., and Tanaka, C. (1993) *Gene (Amst.)* **132**, 57–66
43. Wakatsuki, T., and Hatayama, T. (1998) *Biol. Pharm. Bull.* **21**, 905–910
44. Hatayama, T., Yamagishi, N., Minobe, E., and Sakai, K. (2001) *Biochem. Biophys. Res. Commun.* **288**, 528–534
45. Yamagishi, N., Nishihori, H., Ishihara, K., Ohtsuka, K., and Hatayama, T., (2000) *Biochem. Biophys. Res. Commun.* **272**, 850–855
46. Michels, A. A., Kanon, B., Konings, A. W. T., Ohtsuka, K., Bensaude, O., and Kampinga, H. H. (1997) *J. Biol. Chem.* **272**, 33283–33289
47. Merry, D. E., Kobayashi, Y., Bailey, C. K., Taye, A. A., and Fischbeck, K. H. (1998) *Hum. Mol. Genet.* **7**, 693–701
48. Honda, K., Hatayama, T., and Yukioka, M. (1989) *Biochem. Biophys. Res. Commun.* **160**, 60–66
49. Katsuno, M., Adachi, H., Kume, A., Li, M., Nakagomi, Y., Niwa, H., Sang, C., Kobayashi, Y., Doyu, M., and Sobue, G. (2002) *Neuron* **35**, 843–854
50. Rüdiger, S., Buchberger A., and Bukau, B. (1997) *Nat. Struct. Biol.* **4**, 342–349
51. Bukau, B., and Horwich, A. L. (1998) *Cell* **92**, 351–366
52. Freeman, B. C., Myers, M. P., Schumacher, R., and Morimoto, R. I. (1995) *EMBO J.* **14**, 2281–2292
53. McCampbell, A., Taylor, J. P., Taye, A. A., Robitschek, J., Li, M., Walcott, J., Merry, D., Chai, Y., Paulson, H., Sobue, G., and Fischbeck, K. H. (2000) *Hum. Mol. Genet.* **9**, 2197–2202
54. Steffan, J. S., Kazantsev, A., Spasic-Boskovic, O., Greenwald, M., Zhu, Y. Z., Gohler, H., Wanker, E. E., Bates, G. P., Housman, D. E., and Thompson, L. M. (2000) *Proc. Natl. Acad. Sci. U. S. A.* **97**, 6763–6768
55. Kazantsev, A., Preisinger, E., Dranovsky, A., Goldgaber, D., and Housman, D. (1999) *Proc. Natl. Acad. Sci. U. S. A.* **96**, 11404–11409
56. Boutell, J. M., Thomas, P., Neal, J. W., Weston, V. J., Duce, J., Harper, P. S., and Jones, A. L. (1999) *Hum. Mol. Genet.* **8**, 1647–1655
57. Shimohata, T., Nakajima, T., Yamada, M., Uchida, C., Onodera, O., Naruse, S., Kimura, T., Koide, R., Nozaki, K., Sano, Y., Ishiguro, H., Sakoe, K., Ooshima, T., Sato, A., Ikeuchi, T., Oyake, M., Sato, T., Aoyagi, Y., Hozumi, I., Nagatsu, T., Takiyama, Y., Nishizawa, M., Goto, J., Kanazawa, I., Davidson, I., Tanese, N., Takahashi, H., and Tsuji, S. (2000) *Nat. Genet.* **26**, 29–36
58. Yasuda, S., Inoue, K., Hirabayashi, M., Higashiyama, H., Yamamoto, Y., Fuyuhiro, H., Komure, O., Tanaka, F., Sobue, G., Tsuchiya, K., Hamada, K., Sasaki, H., Takeda, K., Ichijo, H., and Kakizuka, A. (1999) *Genes Cells* **4**, 743–756

Neurochemical Research, Vol. 28, No. 6, June 2003 (© 2003), pp. 839–846

Caspase-1 and -3 mRNAs Are Differentially Upregulated in Motor Neurons and Glial Cells in Mutant SOD1 Transgenic Mouse Spinal Cord: A Study Using Laser Microdissection and Real-Time RT-PCR

Yoshio Ando,[1] Yideng Liang,[1] Shinsuke Ishigaki,[1] Jun-ichi Niwa,[1] Yuemei Jiang,[1] Yasushi Kobayashi,[1] Masahiko Yamamoto,[1] Manabu Doyu,[1] and Gen Sobue[1,2]

(Accepted November 14, 2002)

Amyotrophic lateral sclerosis is characterized by selective motor neuron degeneration. An apoptotic pathway is thought to be involved. It is difficult, however, to analyze the molecular pathogenic mechanism in single motor neurons because of complexity in the neural tissue, which consists of multiple lineages of cells neighboring motor neurons. We quantified the caspase-1 and -3 mRNA in single motor neurons and neighboring glial cells isolated from the spinal ventral horn of mutant SOD1 transgenic (Tg) mice and littermates. Motor neurons and neighboring glial cells were isolated from spinal sections by laser microdissection, and the mRNAs were quantified by RT-PCR. In the Tg mice, caspase-1 mRNA was first upregulated in motor neurons and second in glial cells. The caspase-3 mRNA was increased in motor neurons following the caspase-1 mRNA. These results indicated that caspase-1 and -3 mRNAs are differentially upregulated in motor neurons and glial cells of the Tg mice, and that mRNAs in isolated cells can be accurately assessed using our procedures.

KEY WORDS: Amyotrophic lateral sclerosis (ALS); caspase; laser microdissection; single motor neurons; single glial cells.

INTRODUCTION

Amyotrophic lateral sclerosis (ALS) is a progressive paralytic disorder characterized by selective motor neuron degeneration (1–3). The pathogenic mechanisms remain largely unknown, but mutations in copper/zinc superoxide dismutase (SOD1) genes have been identified in a subpopulation of familial ALS (4,5). Transgenic (Tg) mice expressing mutant SOD1 (mSOD1) have been generated, which develop the clinical and pathological features of ALS. Their analysis would provide a deeper understanding of motor neuron degeneration.

The analysis of cell-type specific (e.g., motor neuron vs. Glial cell) alterations of the mRNA expression is a promising strategy for ALS research. The analysis could enable us to understand a mechanism of motor neuron degeneration in ALS, as well as mSOD1 Tg mice. However, detecting the cell-type–specific gene expression of spinal motor neurons in spinal cord homogenates is difficult, because multiple lineages of cells neighboring motor neurons may conceal changes in the motor neurons. Alterations in the gene expression of isolated degenerating motor neurons should be analyzed. We applied laser microdissection (laser microbeam microdissection and laser pressure catapulting),

[1] Department of Neurology, Nagoya University Graduate School of Medicine, 65 Tsurumai-cho, Showa-ku, Nagoya 466-8550, Japan.
[2] Address reprint requests to: Gen Sobue, MD, Department of Neurology, Nagoya University Graduate School of Medicine, 65 Tsurumai-cho, Showa-ku, Nagoya 466-8550, Japan. Tel: +81-52-744-2385; Fax: +81-52-744-2384; E-mail: sobueg@med.nagoya-u.ac.jp

0364-3190/03/0600-0839/0 © 2003 Plenum Publishing Corporation

which allows target cells from tissue sections to be examined with a minimum of contamination from neighboring cells and surrounding stroma, thus dissolving the problems of tissue complexity. Further we used real-time TaqMan RT-PCR to quantify the mRNA expression levels of isolated target cells.

Here we describe the results of estimating the sequential alteration of caspase-1 and -3 gene expression in isolated spinal motor neurons and in neighboring cells of mSOD1 Tg mice.

EXPERIMENTAL PROCEDURE

Isolation of Single Motor Neurons and Neighboring Cells from Mouse Spinal Cords. We used lumbar spinal cords of three Tg male mice expressing the human SOD1 gene with a G93A mutation that were obtained from Jackson Laboratories (Bar Harbor, ME, USA) and three littermate mice at 8 weeks of age (nonsymptomatic stage, no motor neuron loss), 11 weeks of age (presmptomatic stage, a little motor neuron loss), and 14 weeks of age (symptomatic stage, marked motor neuron loss), respectively. Time course of motor function and histological changes in our mSOD1 (G93A) Tg mice were almost the same as in the previously described research (6). The mice were sacrificed under deep anesthesia according to the guidelines of the Ethical Committee of the Animal Experimental Center, Nagoya University Graduate School of Medicine. Quick-frozen tissues from the mouse lumbar spinal cords were cut on a cryostat into sections 10-μm thick and mounted on a specifically designed 6-μm polyester membrane (PALM, Wolfratshausen, Germany) attached to 0.17-mm-thick glass slides. After staining with Harris's hematoxylin, the sections were washed in RNase-free water and dried (7–9). Regarding RNA quality, we extracted RNA from parts of quick-frozen spinal cords, then electrophoresed them in denaturing gel. Each sample showed 1.5–2.0 at 18S RNA/28S RNA rate, indicating nondegraded RNA (10). The glass slides were positioned on the microscope slide stage of a PALM Laser-MicroBeam System (PALM). The targeted motor neurons and neighboring cells in the spinal ventral horn were selected under the microscope based on morphological criteria. The pulsed laser microbeam cut precisely around the targeted cells (laser microbeam microdissection). Each laser-isolated specimen was subsequently ejected from the glass slide with a single or several laser shots and collected directly into the cap of a PCR tube by a process of laser pressure catapulting in the totally "noncontact" manner previously described (8). We applied these procedures, laser microbeam microdissection, and laser pressure catapulting for the purpose of laser microdissection.

RT-PCR to Detect Cell-Type–Specific-Marker mRNA Levels. Total RNA in the laser-isolated specimen was extracted and digested with DNase to remove contamination genomic DNA using a StratAPrep Total RNA Microprep Kit (Stratagene, La Jolla, CA, USA) according to the manufacturer's instructions. RT-PCR reactions proceeded in a total volume of 50 μl, containing 25 μl of 2 × ThermoScript Reaction Mix, 1 μl of ThermoScript Plus/Platinum Taq Mix (Platinum Quantitative RT-PCR ThermoScript One-Step System, Life Technologies), 40 U of RNaseOUT (Life Technologies), 0.2 mM of each primer, total RNA from the isolated cells, and DNase- and RNase-free water for dilution. The conditions of one-step RT-PCR were as follows: 30 min at 50°C, 5 min at 95°C, then 30 cycles of amplification for 1 min at 95°C, 1 min at 60°C, and 1 min at 72°C. The primer sequences were as follows (gene name, Genbank accession number, amplicon size, forward primer, reverse primer):

choline acetyltransferase (ChAT) as a marker of neurons, D12487, 202,
5′-TGCAACACCTGGTACCTGAA and 5′-GCAGGGCTAGAG TTGACTGG;
glial fibrillary acidic protein (GFAP) as a marker of astrocytes, K01347, 198,
5′-TCCTTCCAAGGTTGTCCATC and 5′-CCAATCAGCCTCA GAGAAGG;
glyceraldehyde-3-phosphate dehydrogenase (GAPDH), M32599, 207,
5′-AAGGGCTCATGACCACAGTC and 5′-ACACATTGGGGGTA GGAACA.

Real-Time TaqMan RT-PCR to Quantify Caspase-1 and -3 mRNA Levels. Total RNA in the laser-isolated specimen containing about 60 motor neurons or about 600 neighboring glial cells, was extracted as described above. These extracted total RNAs were divided into three PCR tubes containing about 20 motor neurons or about 200 neighboring glial cells per PCR tube, respectively, and then GAPDH and caspase-1 and -3 mRNA were measured simultaneously. Real-time TaqMan RT-PCR was performed using the iCycler iQ Real-Time PCR Detection System (BIO-RAD Laboratories, Hercules, CA, USA). RT-PCR reaction mixture was composed as described above (except for adding 0.2 mM of TaqMan probe). The conditions of one-step RT-PCR were as follows: 30 min at 50°C, 5 min at 95°C, then 50 cycles of amplification for 15 sec at 95°C and 1 min at 60°C. Additional reactions were performed on each 96-well plate using known dilutions of cDNA as a template to allow construction of a standard curve relating threshold cycle (Ct) to template mole. This template cDNA was prepared by performing PCR on the outer region of the TaqMan PCR amplicons as previously described (11). The primers sequences were as follows (gene name, Genbank accession number, amplicon size, forward primer, reverse primer):

caspase-1, U04269, 596,
5′-TACCTGGCAGGAATTCTGGA and 5′-ATGATCACCTTGGG CTTGTC;
caspase-3, U19522, 616,
5′-TGGGCCTGAAATACCAAGTC and 5′-CACCCCCAATCAT TCCTCTA;
GAPDH, M32599, 557,
5′-ATCACTGCCACCCAGAAGAC and 5′-TGTGAGGGAGAT GCTCAGTG.

According to the manufacturer's directions, the Ct and the standard curve were calculated using iCycler iQ Real-Time PCR Detection System software (BIO-RAD Laboratories). Threshold line was set at 10 times the standard deviation above the mean baseline fluorescence for PCR cycle 2–20. PCR cycle number at threshold line is represented as Ct. Primer and probe sets were designed from sequences in the Genbank database using Primer Express Software program (Perkin-Elmer Applied Biosystems, Foster City, CA, USA), as follows (gene name, Genbank accession number, amplicon size, forward primer, reverse primer, TaqMan probe):

caspase-1, U04269, 143,
5′-CCCTCAAGTTTTGCCCTTTAGA and 5′-CCCTCGGAGAAA GATGTTGAAA,
5′-TGAATACAACCACTCGTACACGTCTTGCCC;
caspase-3, U19522, 102,
5′-CGTGGTTCATCCAGTCCCTTT and 5′-ATTCCGTTGCCACC TTCCT,

5'-CATGCTGAAGCTGTACGCGCACAA;
GAPDH, M32599, 116,
5'-CCTGGAGAAACCTGCCAAGTAT and 5'-TGAAGTCGCA GGAGACAACCT,
5'-CATCAAGAAGGTGGTGAAGCAGGCATC.

The TaqMan probes contain the fluorophore 5' FAM (6-carboxyfluorescein) as a reporter and 3' TAMRA (6-carbosytetramethylrhodamine) as a quencher. We confirmed that none of the samples were detectable during RT-PCR without RT. Caspase-1 and -3 mRNA levels were normalized to mRNA levels of a housekeeping gene, GAPDH, which was documented to be appropriate as a control for RNA in brain tissue using real-time TaqMan RT-PCR (12).

Data Analysis. Results are expressed as the means ± SEM of at least three independent experiments conducted in triplicate in each group. Statistical differences between individual groups was evaluated by the Kruskal-Wallis test, followed by Scheffe's posthoc test, and were considered significant when $P < .05$.

Immunohistochemical Analysis. Cryostat sections of 5-μm thickness were fixed in cold acetone, air dried, and then processed for immunostaining as described previously (13). After incubation with a rabbit polyclonal antibody against caspase-1 (Santa Cruz Biotechnology, Santa Cruz, CA, USA) or anticleaved caspase-3 rabbit polyclonal antibody (TRAVIGEN, Gaithersburg, MD, USA) in 0.02 M PBS (pH 7.4) at 4°C overnight, bound antibodies were detected by the avidin-biotin-peroxidase (ABC) method, using Vectastain Kits (Vector Laboratory Inc., Burlingame, CA, USA) followed by counterstaining with methyl green, as described previously (14).

RESULTS

Single motor neurons and neighboring cells were isolated from the spinal ventral horn of the mSOD1 Tg mice and the littermates using PALM (Fig. 1A–H). Sections were stained with Harris's hematoxylin (Fig. 1A and E). Margins of motor neurons were dissected by the laser beam (Fig. 1B and F). Motor neurons were isolated from slides by the laser beam (Fig. 1C and G). Neighboring cells were also isolated (Fig. 1D and H). To assess the isolation of motor neurons and neighboring cells (morphologically consisting mainly of glial cells [astrocytes] but excluding neurons), we carried out

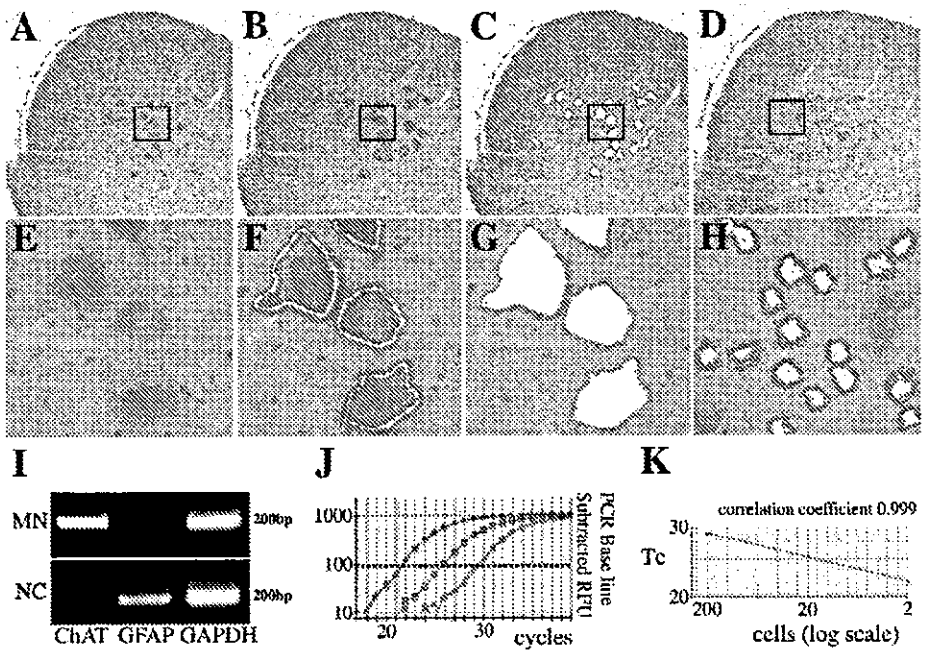

Fig. 1. Qualification and microdissection of target cell profiles. (A–H) Microdissection of motor neurons and neighboring cells in spinal ventral horn. Sections were stained with Harris's hematoxylin (A and E); margins of motor neurons were dissected by the laser beam (B and F); motor neurons (C and G) and neighboring cells (D and H) were isolated from slides by laser pressure catapulting; (E–H) increased magnification of open squares in (A–D). (I) Agarose gel electrophoresis of fragments stained with ethidium bromide after PCR amplification of ChAT, GFAP and GAPDH. Specimen was acquired by laser microdissection of motor neurons (MN) and neighboring cells (NC). (J) GAPDH amplification plots of isolated motor neurons of 200, 20 and 2 cells (starting from the left to right) in duplicate. Dotted line represents threshold line. (K) Standard curve of isolated motor neurons of 200, 20, and 2 cells.

RT-PCR of cell-type–specific markers. The isolated motor neurons expressed the RT-PCR product of ChAT as a marker of motor neurons (15), but not of GFAP as a marker of astrocytes (16) on agarose gel electrophoresis. The isolated neighboring cells expressed the RT-PCR product of GFAP, but not of ChAT (Fig. 1I). These morphological and specific marker assessments confirmed that motor neurons and neighboring cells were definitely isolated. To confirm the linearity of PCR amplification using RT-PCR, we quantified the mRNA derived from 2, 20, and 200 isolated motor neurons. The GAPDH mRNA levels in these cells were proportional to the threshold cycles (Fig. 1J and K), indicating that even these small amounts of RNA were accurately quantified. These results showed that the combination of target cells isolated by laser microdissection and RT-PCR could precisely quantify the level of gene expression in target cells.

Next, we quantified caspase-1 and -3 mRNA derived from about 20 motor neurons and about 200 neighboring cells isolated from the mSOD1 Tg mice and littermates. Using the materials of these small quantities, we could almost constantly measure GAPDH and caspase-1 and -3 mRNA level. In motor neurons isolated from mSOD1 Tg mice, the caspase-1 mRNA level was increased at 11 (presymptomatic stage) and 14 weeks (symptomatic stage) of age (Fig. 2G) compared with age-matched littermates, and the caspase-3 mRNA level was not upregulated at 11 weeks (presymptomatic stage) of age, but increased at 14 weeks (symptomatic stage) of age (Fig. 2H). The caspase-3 mRNA was upregulated later than the caspase-1 mRNA in the motor neurons. In neighboring cells of mSOD1 Tg mice, caspase-1 and -3 mRNA levels had no change at 8 (nonsymptomatic stage) and 11 weeks (presymptomatic stage) of age, but were upregulated at 14 weeks (symptomatic stage) of age (Fig. 2I and J) compared with age-matched littermates. The caspase-1 mRNA was increased in the motor neurons earlier than in the neighboring cells. We showed that caspase-1 amplification plots in the motor neurons at 8, 11, and 14 weeks of age (Fig. 2A–C) and in the neighboring cells at 8, 11, and 14 weeks of age (Fig. 2D–F) when Ct values of the GAPDH amplification plots in mSOD1 Tg mice were almost identical to those in littermates. In the littermates, caspase-1 and -3 mRNA levels have no significant change at the each age.

In addition, we carried out an immunohistochemical analysis for caspase-1 and -3. In motor neurons of mSOD1 Tg mice, caspase-1 immunoreactivity was barely detectable or just above background at 8 weeks of age (Fig. 3A), and was present at 11 and 14 weeks of age (Fig. 3B and C). In neighboring cells of mSOD1 Tg mice, caspase-1 immunoreactivity was present only at 14 weeks of age in neighboring cells (Fig. 3F). In mSOD1 Tg mice, caspase-3 immunoreactivity was detectable in motor neurons and neighboring cells at 14 weeks of age (Fig. 3I and L), while barely observed in motor neurons and neighboring cells at 8 and 11 weeks of age (Fig. 3G, H, J, and K). Caspase-1 and -3 immunoreactivity in motor neurons of littermates was very weak at 8, 11, and 14 weeks of age and almost negative in neighboring cells at all ages (data not shown).

DISCUSSION

Some of the mechanical techniques for microdissection have been developed to isolate cells for analysis from histological section, such as ultrasonically oscillating needle and piezo-driven micropipette (17), laser-assisted cell picking (18), and laser capture microdissection (19). We isolated motor neurons and neighboring cells from spinal cord sections using laser microbeam microdissection and laser pressure catapulting. This procedure is a noncontact technique like laser microdissection, reported by Emmert-Buck et al., that can isolate target cells from tissue sections with minimal risk of contamination from adjacent tissues and cells. However, the amount of RNA obtained from a microdissected specimen is very small. Tissue localization of mRNA expression and changes has been traditionally studied using Northern blot analysis, competitive PCR, in situ hybridization, or RNase protection assays. Although these techniques have proven successful and reliable, they can require large amounts of RNA and can be difficult to optimize and quantify. On the other hand, RT-PCR is very sensitive and allows quantification of a small amount of RNA. Our present procedure combining microdissection and RT-PCR was thought to be very effective to quantify the small amount of mRNA of each adjacent cell. We could reliably quantify mRNA expression from at least two isolated neurons and successfully measure genes of low-level expression such as caspases from isolated 20 neurons.

The present study indicated that caspase-1 and -3 mRNA levels are upregulated in the spinal cord of the mSOD1 Tg mice, findings that are in agreement with studies of spinal cord homogenates of symptomatic mSOD1 (G93A) Tg mice (20–23). We further examined caspase-1 and -3 mRNA levels in specific cells. In motor neurons isolated from mSOD1 Tg mice, caspase-1 and -3 mRNA levels were first increased at 11 and 14 weeks of age, respectively. Caspase-1 mRNA